

PUERTO RICO DEPLOYABLE RADAR NETWORK DESIGN; SITE SURVEY AND RADAR DESIGN

by

Jorge M. Trabal-del Valle

A thesis submitted in partial fulfillment of the requirements for the degree of

MASTER OF SCIENCE
in
ELECTRICAL ENGINEERING

UNIVERSITY OF PUERTO RICO
MAYAGÜEZ CAMPUS
2003

Approved by:

Sandra L. Cruz-Pol, PhD
Member, Graduate Committee

Date

Rafael Rodríguez-Solís, PhD
Member, Graduate Committee

Date

José Colom-Ustáriz, PhD
President, Graduate Committee

Date

Fernando Gilbes, PhD
Representative of Graduate Studies

Date

José L. Cruz-Rivera, PhD
Chairperson of the Department

Date

ABSTRACT

The Microwave Remote Sensing Laboratory (MIRSL) at the University of Massachusetts at Amherst and the Clouds Microwave Measurements of Atmospheric Events (CLiMMATE) Laboratory at the University of Puerto Rico at Mayagüez are collaborating to modify marine radars for use as meteorological radar nodes in a proposed weather radar network. This will be the first network to measure lower atmospheric phenomena in Puerto Rico. The radar consists of an antenna, a rotator, and a transceiver placed at the top of a tower or building, along with a data processing system. This thesis describes the survey method used in the MIRSL Tilson Farm field site, and the eleven campuses of the University of Puerto Rico backbone and justifies their fixed offset antennas' elevation angle and location. A new dual-polarization X-band Doppler radar modification design with an internal calibration loop and a method to stabilize the magnetron thermal frequency drift is also described.

RESUMEN

El “*Microwave Remote Sensing Laboratory (CPRS)*” localizado en la Universidad de Massachussets en Amherst y el “*Clouds Microwave Measurements of Atmospheric Events Laboratory (CLiMMATE)*” localizado en el Recinto Universitario de Mayagüez están trabajando en la modificación de radares marinos que serán usados como nodos en una red de radares climatológicos. Esta será la primera red de radares para medir los fenómenos atmosféricos ocurrentes en la atmósfera baja en Puerto Rico. El radar consiste de una antena, un mecanismo rotativo, y un transmisor y un receptor que serán colocados sobre una torre o un edificio en compañía del sistema procesador de datos. Esta tesis describe el método de estudio de campo (“survey”) utilizado en el “*MIRSL Tilson Farm*” y los once recintos que componen la Universidad de Puerto Rico y justifica para cada uno el ángulo de elevación de la antena requerido para sobrepasar los obstáculos, y su localización. El nuevo diseño modificado del radar Doppler, polarimétrico, Banda X con un lazo interno para la calibración interna y un banco de filtros Gaussianos para corregir la variación de frecuencia debido a cambios termales en el magnetrón es también explicado.

To my family ...

ACKNOWLEDGMENTS

First I would like to thank God for giving me the life and mind to work in this research and finish my thesis. I would like to thank my advisors José Colom, Sandra Cruz and Stephen Sekelsky for the time they spent supporting and guiding me during my thesis work. Thanks also to the other member of the committee, Rafael Rodriguez.

I'd like to thank the people from the Cloud Microwave Measurements of Atmospheric Events (CLiMMATE) Laboratory at the University of Puerto Rico at Mayagüez and the Microwave Remote Sensing Laboratory (MIRSL) at the University of Massachusetts at Amherst for teaching me the first steps of my research, especially to Leyda Leon, Harry Figueroa, Jorge Román, Eric Knapp and Ninoslav Majurec.

I am very thankful for the opportunity that was given to me for two summers by the Northeast Alliance Summer Program for Undergraduate Research under the command of Director Dr. Ann Lewis and Coordinator Stephanie Burrell to work at MIRSL.

Thanks to the NASA Partnership for Spatial and Computational Research (PaSCoR) Laboratory at University of Puerto Rico at Mayagüez, especially to the administrator Roy Ruiz for helping me to digitally locate in space the measured points for the antenna locations.

My acknowledgments to our sponsors: NASA Tropical Center for Earth and Space Studies (TCESS) and NASA Faculty Award for Research in Cloud Microwave Measurements of Atmospheric Events (FAR-CLiMMATE) for trusting us and giving us funding to make the research possible.

Finally, I want to thanks my family especially my parents for their support, and my girlfriend Ibis Benito for being at my side always and serving as my survey partner and spelling corrector.

TABLE OF CONTENTS

	Page
LIST OF TABLES	viii
LIST OF FIGURES	ix
CHAPTER 1 INTRODUCTION.....	1
1.1 Motivation.....	1
1.2 Objectives.....	2
1.3 Literature review.....	3
1.4 Summary of chapters	7
CHAPTER 2 CURVED EARTH EFFECT AND TILSON FARM SURVEY	9
2.1 Introduction	9
2.2 Curved Earth effect.....	9
2.3 Tilson Farm survey materials and procedure	15
2.4 Survey results and discussion.....	16
CHAPTER 3 RADAR NETWORK SITE SURVEY.....	22
3.1 Introduction	22
3.2 Survey procedure and materials	23
3.3 Survey results and discussion.....	24
3.3.1 Aguadilla Campus	24
3.3.2 Arecibo Campus.....	26
3.3.3 Bayamón campus	28
3.3.4 Carolina campus.....	30
3.3.5 Cayey campus	32
3.3.6 Humacao campus	34
3.3.7 Mayagüez campus	36
3.3.8 Medical Sciences campus	38
3.3.9 Ponce Campus.....	40
3.3.10 Río Piedras campus	42
3.3.11 Utuado campus.....	45
3.4 Radar network coverage.....	47
3.4.1 Maximum range definition	47
3.4.2 Campuses coverage representation	49

CHAPTER 4 NETWORK RADAR DESIGN.....	55
4.1 Overview	55
4.2 Transceiver	56
4.2.1 System description	57
4.2.2 System specifications	59
4.3 Magnetron thermal frequency drift control method	62
4.4 Internal calibration.....	65
CHAPTER 5 CONCLUSIONS AND FUTURE WORK.....	69
5.1 Summary	69
5.2 Future work	70
REFERENCES.....	71
BIBLIOGRAPHY	73
APPENDIX A SURVEYED CAMPUSES LOCATION.....	74
APPENDIX B CAMPUSES SURVEY DATA.....	86
APPENDIX C RADAR PARTS SPECIFICATIONS SUMMARY.....	98

LIST OF TABLES

Table	Page
2.1	Obstructions data for Tilson Farm site survey..... 18
2.2	Minimum obstruction free view angles 19
3.1	Antenna tower and maximum range for a 1° antenna inclination angle 52
4.1	Calibration loop specifications 67
B.1	Aguadilla campus survey data 87
B.2	Arecibo Campus survey data 88
B.3	Bayamón campus survey data..... 89
B.4	Carolina campus survey data 90
B.5	Cayey campus survey data 91
B.6	Humacao campus survey data 92
B.7	Mayagüez campus survey data..... 93
B.8	Medical Sciences campus survey data..... 94
B.9	Ponce campus survey data 95
B.10	Río Piedras campus survey data 96
B.11	Utua campus survey data 97
C.1	Radar parts specifications summary 99

LIST OF FIGURES

Table	Page
1.1 Simultaneous differential polarimetric block diagram [7]	7
2.1 Flat Earth problem for weather radar	10
2.2 Curved Earth problem for weather radar	11
2.3 Plot of h1 equation	12
2.4 Plot of h2 equation	13
2.5 Plot of h + dh	14
2.6 Survey Instruments	16
2.7 Tilson Survey Data Plot (H=3.66 m)	17
2.8 Antenna Beam Obstruction	18
2.9 Tilson Survey Data Plots (H=3.66 m and H=14.02 m)	20
3.1 Aguadilla campus survey data plot and site panorama	25
3.2 Aguadilla campus maximum range plot with a 3.4° tilted beam	26
3.3 Arecibo campus survey data plot and site panorama	27
3.4 Arecibo campus maximum range plot with a 3.3° tilted beam	28
3.5 Bayamón campus survey data plot and site panorama	29
3.6 Bayamón campus maximum range plot with a 5° tilted beam	30
3.7 Carolina campus survey data plot and site panorama	31
3.8 Carolina campus maximum range plot with a 14.1° tilted beam	32
3.9 Cayey campus survey data plot and site panorama	33
3.10 Cayey campus maximum range plot with a 16° tilted beam	34
3.11 Humacao campus survey data plot and site panorama	35
3.12 Humacao campus maximum range plot with a 6° tilted beam	36
3.13 Mayagüez campus survey data plot and site panorama	37
3.14 Mayagüez campus maximum range plot with a 4.8° tilted beam	38
3.15 Medical Sciences campus survey data plot and site panorama	39
3.16 Medical Sciences campus maximum range plot with a 3.5° tilted beam	40
3.17 Ponce campus survey data plot and site panorama	41
3.18 Ponce campus maximum range plot with a 5.2° tilted beam	42
3.19 Río Piedras campus survey data plot and site panorama	43
3.20 Río Piedras campus maximum range plot with a 3.3° tilted beam	44
3.21 Utuado campus survey data plot and site panorama	45
3.22 Utuado campus maximum range plot with a 11.3° tilted beam	46
3.23 Vertical height temperature variations in the San Juan area, obtained on March 2003	47
3.24 Radar network coverage using 4 Km height circles.	49
3.25 Radar network coverage using 1 Km maximum height circles.	50

3.26	Radar network coverage using 1 Km maximum height circles and radars at the mountains.	51
3.27	Radar network coverage using 1° antenna elevation angles at the campuses and radars at the mountains.	54
4.1	Raytheon marine radar transceiver	56
4.2	Network radar transceiver block diagram	58
4.3	Radar noise figure calculation elements.....	61
4.4	Plot of the magnetron's thermal frequency-drift	63
4.5	Block diagram for the magnetron thermal-frequency-drift control method....	63
4.6	Gaussian filters representation plot.....	64
4.7	Logarithmic subtraction of the Gaussian filters.....	65
4.8	Internal calibration error plot.....	67
4.9	Radar calibration loop block diagram.....	68
A.1	University of Puerto Rico, Aguadilla Campus. Image from satellite IKONOS.	75
A.2	University of Puerto Rico, Arecibo Campus. Image from satellite IKONOS.	76
A.3	University of Puerto Rico, Bayamón Campus. Image from satellite IKONOS.	77
A.4	University of Puerto Rico, Carolina Campus. Image from satellite IKONOS.	78
A.5	University of Puerto Rico, Cayey Campus. Image from satellite IKONOS. .	79
A.6	University of Puerto Rico, Humacao Campus. Image from satellite IKONOS.	80
A.7	University of Puerto Rico, Mayagüez Campus. Image from satellite Landsat.	81
A.8	University of Puerto Rico, Medical Sciences Campus. Image from satellite Landsat.	82
A.9	University of Puerto Rico, Ponce Campus. Image from satellite IKONOS...	83
A.10	University of Puerto Rico, Río Piedras Campus. Image from satellite IKONOS.....	84
A.11	University of Puerto Rico, Utuado Campus. Image from satellite IKONOS.	85

CHAPTER 1

INTRODUCTION

1.1 Motivation

Distributed, collaborative and adaptive radar network systems (DCAS) are a new weather forecast design approach proposed by the University of Massachusetts at Amherst, the University of Puerto Rico at Mayagüez, Colorado State University and the University of Oklahoma under a new Engineering Research Center (ERC) named CASA (the Center for Collaborative, Adaptive Sensing of the Atmosphere). The new radar systems will be developed to sample the lower atmosphere to accurately detect, monitor and predict extreme weather events. This system will bring us the ability to observe, anticipate, sense, track and predict to act quickly before damage occurs. Most of the atmospheric phenomena events occur at the boundary layer in the lower atmosphere which is virtually unsampled by current observing systems, inhibiting our ability to detect, predict, and respond in anticipation.

Today's atmospheric observation approaches rely on the National Weather Services NEXRAD (next generation weather radar) which is a 10-year old network based on a 50-year old technology, composed of 165 long-range (more than 200 km) Doppler radars in the United States including one in Cayey, Puerto Rico. Other radars are also used by television stations for obtaining and providing information about atmospheric phenomena. The radar sensors have low sensitivity and its long-range limits the resolution. Furthermore, the earth's curvature prevents the lower boundary layer from being observed at far distances from the radar, missing a significant amount of information [1].

Another disadvantage of NEXRAD and other currently utilized weather observation radars is that they transmit only in horizontal polarization mode. With

dual-polarized radars, it is generally possible to achieve higher hydrometeor estimation accuracies and in some cases the hydrometeor amount. The information that can be obtained from dual-polarized radars is so dramatic that it is now considered to be an indispensable tool for the study of the formation and evolution of precipitation [2].

The Earth curvature problem could be resolved and an enhancement in spatial resolution can be achieved with the implementation of a deployable radar network system in Puerto Rico by dispersing the radars with a short range and using low antenna vertical angles (near one degree) to cover the lower atmosphere (below 1 km). The radar system will be a distributed, collaborative and adaptive network to overcome current limitations, where distributed means many sensors dispersed with short range to reduce the Earth curvature problem, collaborative refers to the coordinated targeting of multiple radars and their beams using atmospheric analysis tools (detecting, predicting, and data mining) to concentrate system resources, such as radiated power, bandwidth, and computing cycles, onto important volumes of the atmosphere where threats exist; and adaptive refers to the ability of the network and computing elements to rapidly reconfigure in response to changing conditions. Before the implementation, a site survey must be conducted in order to decide the points where the radar antennas must be installed and also the radar system has to be designed.

1.2 Objectives

The goal of this research is to develop a methodology for conducting site surveys to deploy low-cost, high-resolution weather radar network to measure lower atmospheric phenomena in Puerto Rico. The proposed Network of Radars (NetRad) will serve as a complement to currently used NEXRAD (next generation weather radar). NetRad will overcome the curved earth problem and obtain enhanced spatial resolution. Each of the eleven campuses of the University of Puerto Rico will be

surveyed in order to decide the liability of installing one radar at each the campus' tallest building. In addition, the tallest mountains of the island will be taken into consideration for purpose of coverage in case the campus radars do not provide total island coverage. Each location will be digitally located in space through satellite images and government maps.

As a second goal, a dual-polarization Doppler radar operating in the X-band using the simultaneous transmission method with an orthomode transducer, a magnetron as a power source, and a 360° scanning system would be designed at a block diagram level for the proposed network. The radar will have a feedback loop method to correct the frequency drift in the magnetron caused by the changes in temperature.

1.3 Literature review

Nowadays, ground radars are installed in the highest mountains to get an obstruction-free beam angle view and receive the least scatter possible. Installing meteorological radars at high altitudes causes a loss of important information from the boundary layer or the lower atmosphere. For example, the NEXRAD located in Cayey, Puerto Rico is at a height of 881 meters over sea level, losing important information of the lower atmospheric phenomena. Furthermore the Earth's curvature hides some atmospheric activities from the radar footprint. As previously mentioned, the interest is to study the lower part of the atmosphere which is below 1 km.

The most important weather radar network in the United States and in Puerto Rico (NEXRAD), transmit and receive radio waves with a single, horizontal polarization. One of the most significant advances in radar meteorology since the mid-1970s has been the study of a number of polarimetric techniques for rain retrieval [3]. Examples are the S-band polarimetric radar of the National Severe Storms Laboratory [4], and the millimeter-wave cloud radar of the University of Massachusetts at Amherst [5]. Both horizontal and vertical polarization waves are transmitted in a dual-polarization radar.

Dual or multi-polarization radars have proven to be valuable tools for studying the microstructure of precipitation [6]. They offer several advantages over conventional radars in estimating precipitation types and amounts [3]. These advantages are: the capability to discriminate between hail and rain, detect mixed phase precipitation, and much more accurately estimate rainfall [3][7]. Also the polarimetric measurements are immune to attenuation through heavy precipitation [4]. Dual-polarization radar systems are configured to measure the complex scattering matrix \mathbf{S} , by transmitting horizontally and vertically polarized waves and measuring the magnitude and phase of the horizontal and vertical components of the scattered field [5]. The incident electric field \mathbf{E}^i and scattered electric field \mathbf{E}^s are related to the scattering matrix \mathbf{S} through

$$\begin{bmatrix} E_v \\ E_h \end{bmatrix}^s = \begin{bmatrix} S_{vv} & S_{vh} \\ S_{hv} & S_{hh} \end{bmatrix} \begin{bmatrix} E_v \\ E_h \end{bmatrix}^i \quad (1)$$

where S_{ij} are random variables and correspond to the i^{th} received polarization and j^{th} transmitted polarization [5]. Measurements of the scattering matrix are made on successive transmitted pulses, separated by a time lag equal to the interpulse spacing τ [5].

The well-known meteorological radar parameters derived from these covariances are the horizontal and vertical polarization reflectivity factors Z_h^e and Z_v^e , respectively, differential reflectivity (Z_{dr}), linear depolarization ratio (LDR), copolarized correlation coefficient (ρ_{hv}), and specific differential phase [5]. The parameters are related to the elements of the scattering matrix through

$$Z_h^e = 4 \frac{\lambda^4}{|K|^2 \pi^4} \langle |S_{hh}|^2 \rangle \quad (2)$$

$$Z_v^e = 4 \frac{\lambda^4}{|K|^2 \pi^4} \langle |S_{vv}|^2 \rangle \quad (3)$$

$$Z_{dr} = 10 \log \frac{\langle |S_{hh}|^2 \rangle}{\langle |S_{vv}|^2 \rangle} \quad (4)$$

$$LDR = 10 \log \frac{\langle |S_{vh}|^2 \rangle}{\langle |S_{hh}|^2 \rangle} \quad (5)$$

$$\rho_{hv} = \frac{\langle S_{hh} S_{vv}^* \rangle}{\langle |S_{hh}|^2 \rangle \langle |S_{vv}|^2 \rangle} \quad (6)$$

The equivalent reflectivity factors are good indicators of what polarization is better scattered by the scatterer. Differential reflectivity is a ratio of the reflected horizontal and vertical power returned and it is a good indicator of drop shape and average drop size, therefore very important for accurate precipitation estimation. The correlation coefficient is a correlation between the reflected horizontal and vertical power returned and is a good indicator of regions where there is a mixture of precipitation types, such as rain and snow. Linear depolarization ratio is a ratio of a vertical power returned from a horizontal pulse or a horizontal power returned from a vertical pulse and is a good indicator of regions where a mixture of precipitation types occur. Finally, the specific differential phase is a comparison of the returned phase difference between the horizontal and vertical pulses and is caused by the difference in the number of wave cycles (or wavelengths) along the propagation path for horizontally and vertically polarized waves. It is a propagation effect and is a good estimator of rain rate. Propagation effect refers to the process whereby cloud and

precipitation particles, as a whole, work to modify the power and phase of the transmitted signal.

The use of a polarization switch is a common way to alternate between horizontal and vertical polarizations in each successive pulse. This method of alternating polarization has four drawbacks [7]. First, a long dwell time is needed to obtain estimates with acceptable errors; an active waveguide switch is needed to alternately select horizontally and vertically polarized waves to the antenna feed, which is expensive and difficult to maintain; ground clutter filtering is compromised because it can be best done only on echoes of equal polarization; and, there is considerable attenuation caused by the switch.

The alternating polarization drawbacks can be eliminated using a simultaneous differential polarimetric transmission in an elliptical wave as proposed in [7]. That method will be used in the Puerto Rico deployable radar design. The design was proposed as an implementation to the polarimetric capability of the WSR-88D (NEXRAD) radar [8]. A basic diagram from [7] of the proposed system is shown in Figure 1. The design provides a polarimetric Doppler weather radar system which does not require a high power, high frequency switch. It simultaneously transmits horizontally and vertically polarized waves, without the need to control the phase between the two components.

Using simultaneous transmission eliminates the need for the switch. A switch must be tuned, must have power supplies, is fairly large, and introduces attenuation [7]. For the same error in estimates, the dwell time with simultaneous transmission is shorter than the time needed with alternating transmission [7]. The design requires two identical coherent receivers and if one transmitter is used, the signal to noise ratio in each receiver is reduced by one-half [7].

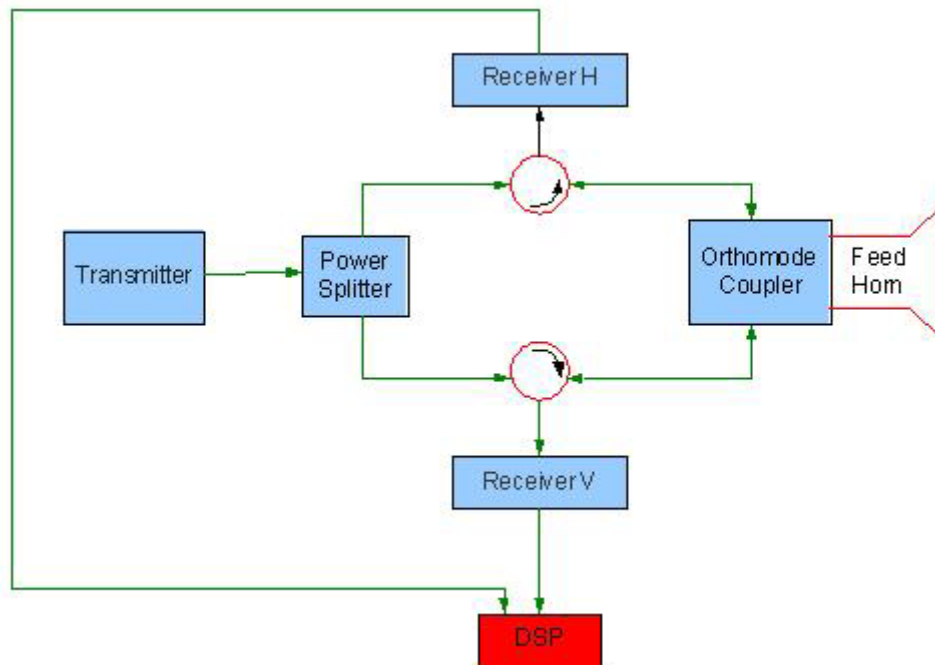


Figure 1.1. Simultaneous differential polarimetric block diagram [7]

1.4 Summary of chapters

Chapter 2 presents the radar beam propagation problem caused by the curvature of the Earth and describes and analyzes the methodology implemented to survey the Tilson farm site for antenna inclination angle and tower requirements.

Chapter 3 is devoted to the Puerto Rico deployable radar network site survey. It discusses the survey procedure and analyzes the data obtained in each of the eleven campuses of the University of Puerto Rico for antenna inclination angle and tower requirements. Puerto Rico maps with the radar backbone coverage are also shown for comparison and visualization purposes.

Chapter 4 describes the polarimetric Doppler radar system at block diagram level intended for use in each node of the deployable radar network. The internal calibration configuration and the Gaussian filter bank method for magnetron

frequency drift control is explained. In addition, components part numbers and costs are shown for the radar.

Chapter 5 summarizes the thesis, and presents conclusions.

CHAPTER 2

CURVED EARTH EFFECT AND TILSON FARM SITE SURVEY

2.1 Introduction

The Cloud Microwave Measurements of Atmospheric Events (CLiMMATE) Laboratory and the Microwave Remote Sensing Laboratory (MIRSL) are collaborating to construct a polarimetric Doppler radar by modifying a Raytheon marine radar to use in a deployable radar network to study the lower atmospheric phenomena and to solve the curved earth propagation problem. In the summer of 2003, MIRSL installed the Raytheon marine radar at the University of Massachusetts, Amherst at the Tilson Farm to collect preliminary measurements.

However, before the measurements were taken, a study of the site and the earth propagation problem was conducted in order to decide the height of the radar tower and the inclination angle the antenna must have, for the beam point above clutter from trees and buildings. Mathematical relationships to describe the curved earth problem and analysis of survey data from the UMass Tilson Farm field site will be discussed.

2.2 Curved Earth effect

If we analyze earth as a flat surface, the propagation of the radar beam may look as in Figure 2.1, where \mathbf{H} is the height of the antenna, \mathbf{R} is the radar horizontal range, θ is the angle between the horizontal radar range and the radar beam, and $\mathbf{h1}$ is the distance between \mathbf{R} and radar beam.

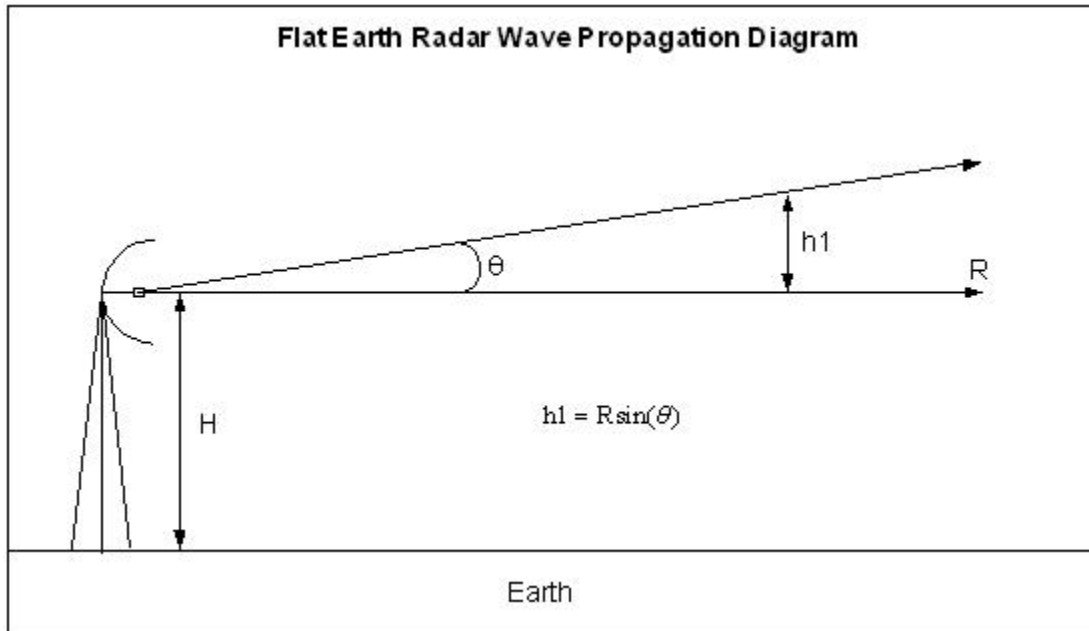


Figure 2.1. Flat Earth problem for weather radar

In this representation the beam height at any distance (range) from the antenna can be obtained from the equation,

$$h1 = R \sin(\theta) + H \quad (2.1)$$

which shows that the beam height only depends on the tilt angle and the antenna height. But this is not a good representation of the propagation problem.

In the real world, the earth has a curvature that affects the range and hides some scatterers from the radar beam or print area [3]. To solve that problem a sketch was created with all the wave propagation, distance parameters, and curved earth effects as shown in Figure 2.2 [9].

In the diagram the letter **h1** is the perpendicular distance from the earth to the radar horizontal range, and **h2** is the distance (aligned with the earth's radius $D/2$ and **h1**) between **R** and radar beam, and **D** is the earth's diameter (12756.272 km).

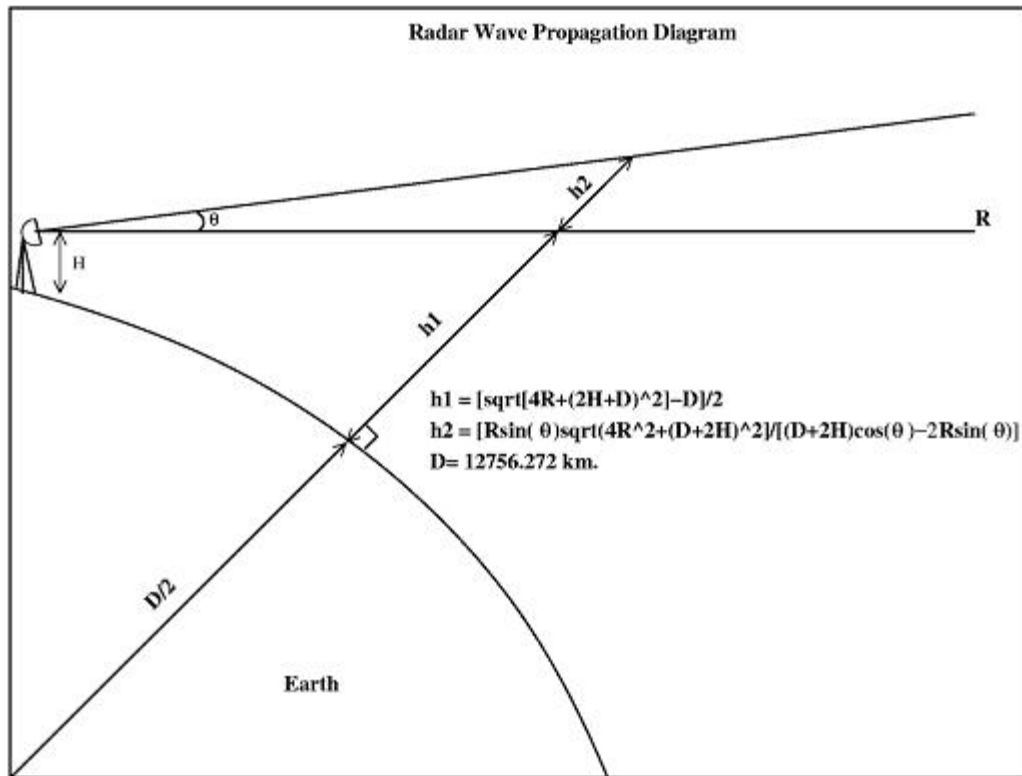


Figure 2.2. Curved Earth problem for weather radar

Having the diagram and all its parameters defined, the known parameters **h1** and **h2** were derived working with the geometry of the problem, obtaining

$$h1 = \frac{[\sqrt{4R + (2H + D)^2} - D]}{2} \quad (2.2)$$

$$h2 = \frac{[R \sin(\theta) \sqrt{4R^2 + (D + 2H)^2}]}{[(D + 2H) \cos(\theta) - 2R \sin(\theta)]} \quad (2.3)$$

It is easy to see from the above equations that both depend on the antenna height **H**, the earth's diameter **D** and the radar range distance **R**. Furthermore, **h2** depends

on the angle between the radar range distance and the radar beam θ . The **h1** equation does not depend on θ because it does not consider the antenna tilt angle.

With these two equations, the behavior of the radar wave on the earth can be plotted. First **h1** vs. the radar range **R** are plotted in Figure 2.3. In the plot, the axes are in logarithmic form and in kilometer units (to better see the shape of the curves) and there are two curves in the same plot. The solid line curve is the **h1** equation plotted assuming that the antenna was at ground level. The dashed curved is the **h1** equation plotted assuming that the antenna was at a height of 14.02 m (12.8 m tower plus 1.22 m from transceiver and the antenna).

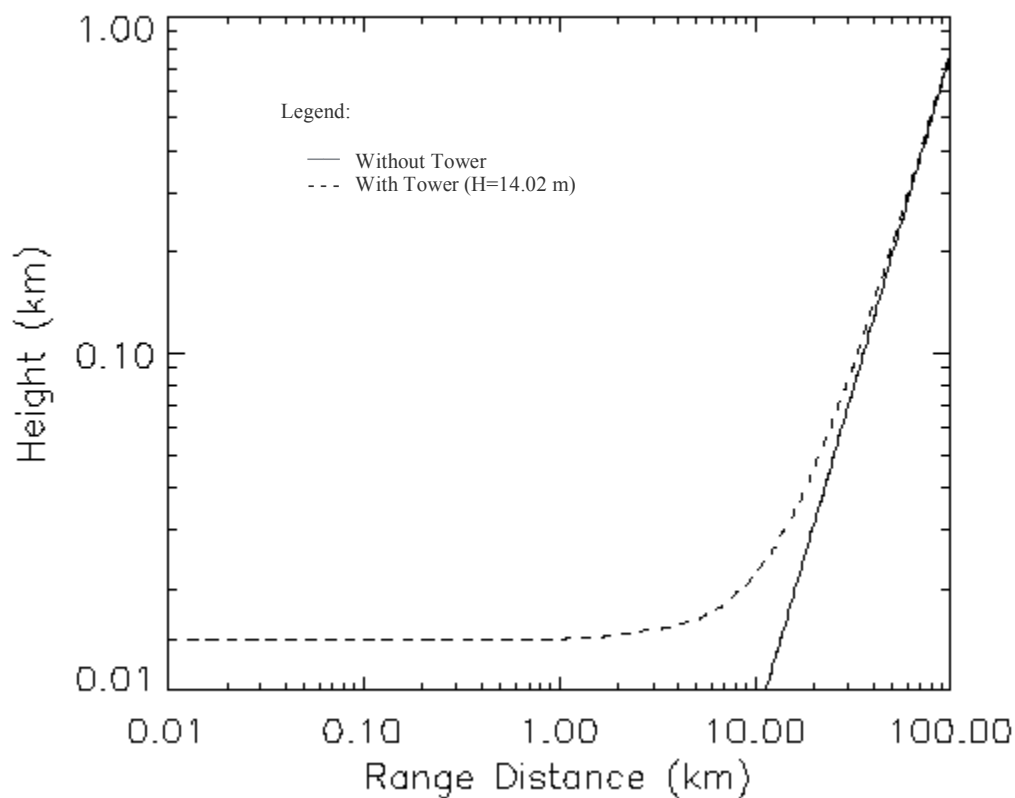


Figure 2.3. Plot of h1 equation

The plot shows that the dashed curve begins at the antenna height, while the solid curve begins at no height and shortly after 30 km both curves look identical because over that point, h_1 is bigger than the antenna height H , causing an insignificant antenna height at large range.

Having described the h plot, the next plot to present is the h_2 plot shown in Figure 2.4, which has the same logarithmic axes and same units, but with different curves that depend on the tilt or vertical angle that the antenna should have to surpass the obstacles. This plot has five different curves at five different tilt angles ranging from one degree to five degrees. From the plot, the height of the radar beam at a specific distance of the antenna compared to the horizontal distance can be obtained. It can be used for the knowledge of the maximum range (distance) the radar beam can reach before the beam enters the ice layer (useless data), which in this case occurs at 3 Km.

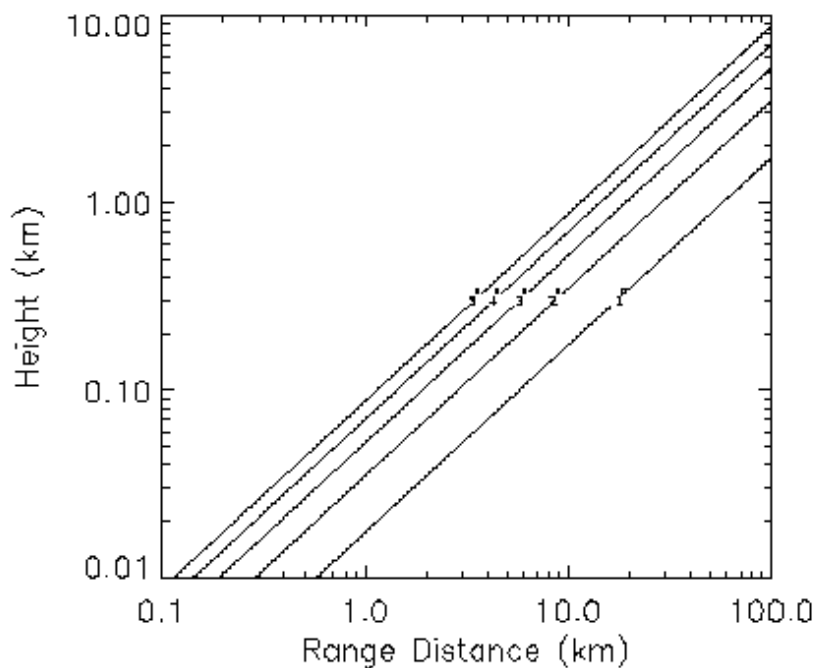


Figure 2.4. Plot of h_2 equation

The plot shows that if the antenna tilt-angle increases, the center of the radar beam will be higher compared with the lower angles. As a consequence, the beam will miss important data close to the Earth's surface. However the use of a larger tilt angle reduces the cost of the radar node by reducing the required tower height, but the beam will reach a higher height at a shorter distance from the antenna and important atmospheric phenomena occurring in the low troposphere would be missed from the radar footprint.

Having plotted the h_1 and h_2 equations, the pertaining plot is the addition of equations 2.2 and 2.3 and plotting against the radar range R in logarithmic axes, which is shown in Figure 2.5. The plot has two curves with the solid curve having no antenna height and tilt angle of five degrees and the dashed curve with antenna height of 14.2 m and same tilt angle. Looking at this plot, the real height at which the radar beam will be from the Earth at a specific distance or range point from the antenna can be determined.

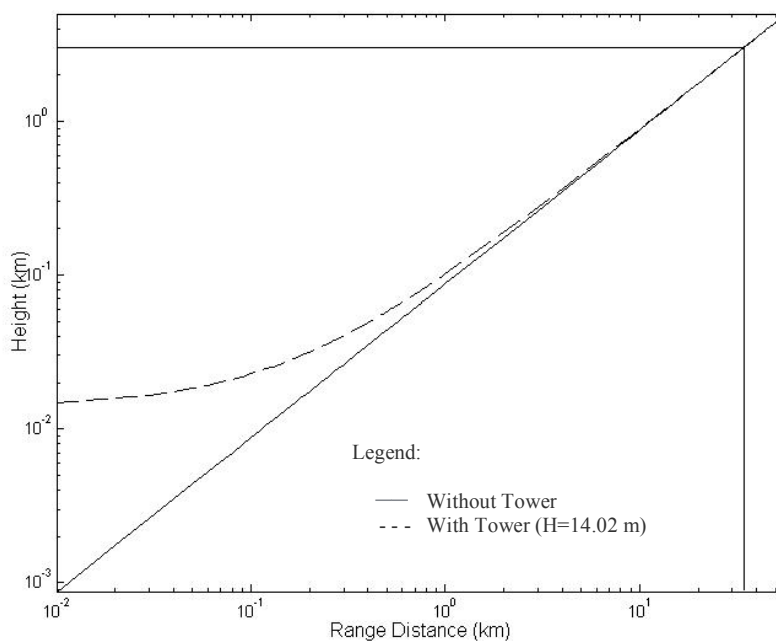


Figure 2.5. Plot of $h + dh$

The plot shows that the dashed curve begins at the antenna height, while the solid curve begins at no height. Also, the two curves behave like one curve after a range distance of 2 km. It is also shown that the curves behave more like the **h2** curve than the **h1** curve, so the antenna tilt angle will affect the height of the beam more than the curve of the Earth. If a lower antenna tilt angle is used, better results can be obtained in the detection of weather signals, but it cannot always be achieved like in the Tilson farm case.

A point where the height of the radar beam is 3 km was marked on the plot to show the height where the ice layer begins. This establishes the radar range; approximately 35 km in the case of a tilt angle of 5°.

2.3 Tilson Farm survey materials and procedure

The first step was to make the decision of which area on the campus the tower must be installed to get an obstruction-free view angle with accessibility to take the measurements. The first tower will be installed at Tilson Farm, therefore this site was assessed first.

To determine the height of the tower and fixed elevation offset of the antenna, the minimum elevation angle over a full 360° azimuth swath was measured in 5° increments from North to West using a distance range meter telescope (model DM-A3 from TOPCON), a digital level (SMART TOOL Builder's Angle Finder) and a compass. The distance range meter telescope is a digital instrument that measures distance and angles with the help of a prism (reflector) and has a telescope which is used to see the obstacles, increasing the zenith angle until they disappear. This angle marks the minimum antenna elevation angle needed to surpass the obstacles in that specific azimuth angle. The digital level is the instrument used to measure the angle and is positioned over the telescope. The compass is a magnetic instrument that

always points to the North Pole and was used to measure the azimuth angles. The survey instruments are shown in the next Figure.

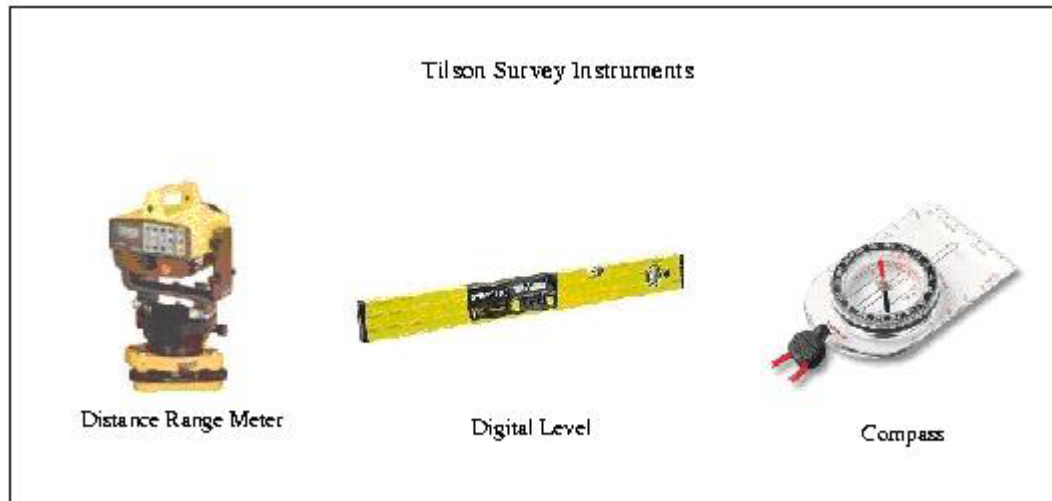


Figure 2.6. Survey Instruments

2.4 Survey results and discussion

A plot of minimum obstruction angle vs. azimuth angle is shown in Figure 2.7. The numbers on the plots and tables, refer to the obstacles in the Tilson farm survey. The plot shows that some minimum angles required to surpass the obstructions (mostly tall trees) at an antenna height of 3.66 m and a 360° azimuth run are very high (over 10°).

The minimum angle requirement is about 5°, which is the limiting angle established by the far hills located from 230° to 260° azimuth angles. This is the limiting angle because to surpass the hill and lower the 5° angle the radar must be very high. For example, assuming that the hill is at a distance of 3.22 km, the antenna height needed to reduce the tilt angle from 5° to 4° is 56.39 m and from 5° to 0° is 281.33 m and this is not acceptable. Therefore, the antenna tilt angle must be 5° or more, considering the lowest possible angle to prevent entering the ice layer (3 km

high) with a small radar range. To achieve a lower tilt angle a tower must be used and some calculations for the nearest (worst) obstructions must be done.

For the purpose of the calculations of the height of the obstructive objects and trees, the distance between the center of the container and the big obstacles was measured and the height h of the obstructions was obtained using the diagram shown in Figure 2.8. The diagram shows the parameters measured at the Tilson farm survey and what the obstructions look like. H is the antenna height, θ is the antenna tilt angle, h is the obstruction height, and d is the distance from the antenna to the obstruction.

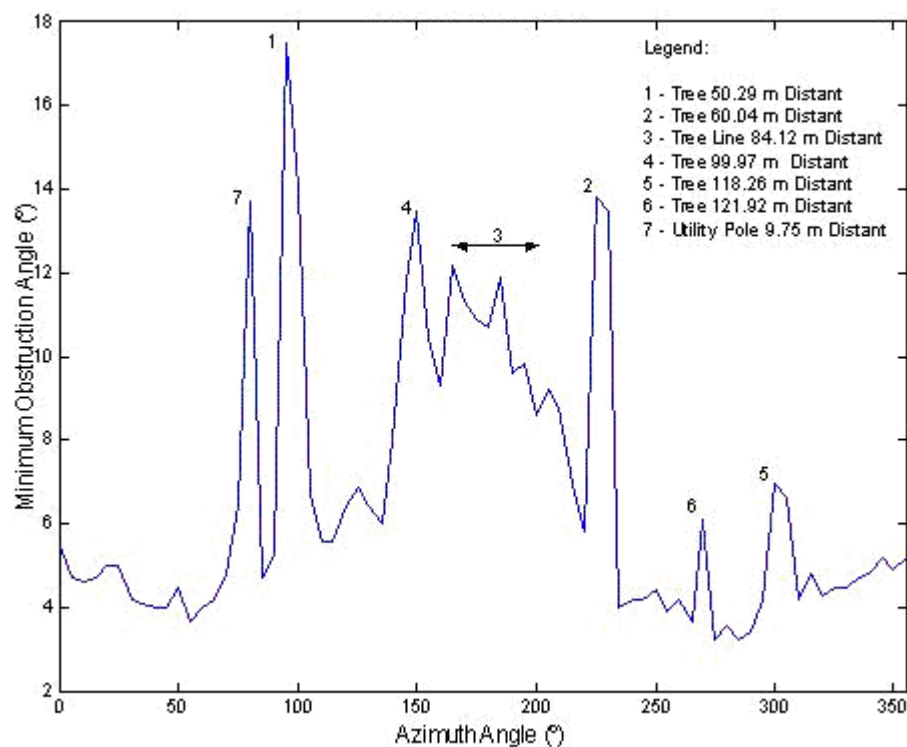


Figure 2.7. Tilson Survey Data Plot ($H=3.66$ m)

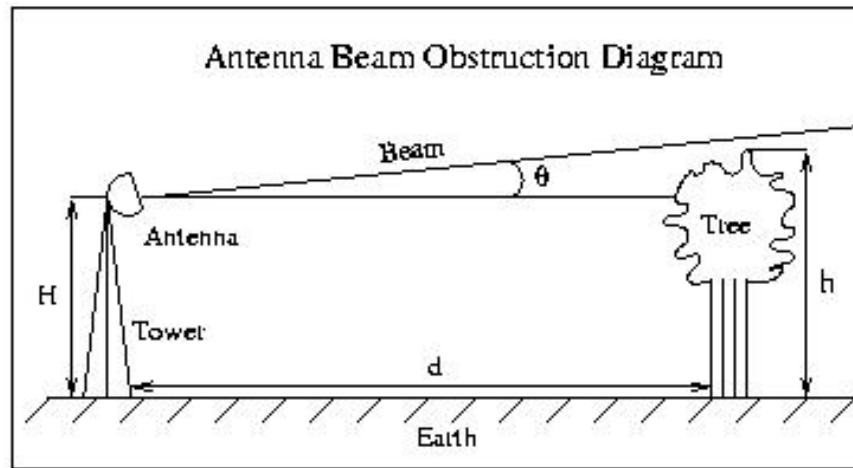


Figure 2.8. Antenna Beam Obstruction

The equation derived to obtain the obstacles' height is

$$h = d \tan(\theta) + 3.66 \quad (2.4)$$

where 3.66 m was added because the measurements were taken at that height. The distances obtained at the survey and the obstructions' heights were estimated using Figure 2.8 and are summarized in Table 2.1.

Table 2.1
Obstructions data for Tilson Farm site survey

Obstruction Description	Distance to Obstruction (m)	Obstruction Height (m)
Tree (1)	50.29	19.51
Tree (2)	60.05	18.4
Tree Line (3)	84.12	21.84
Tree (4)	99.97	26.93
Tree (5)	118.26	18.18
Tree (6)	121.92	16.69
Utility Pole (7)	24.99	9.75

With the distance between the obstructions and the antenna location at hand, the minimum antenna tower height needed to surpass the obstacles from the radar beam with a minimum antenna tilt angle of 5° can be calculated using equation 2.4.

First, using the measured tilt angle needed to surpass the obstacles and the distances between them and the antenna location in equation 2.4, the heights of the obstacles were obtained. Second, using the desired angle of 5° in the equation, the desired obstacle height was calculated. Then, subtracting the required height from the real height gives the desired antenna height to get the required free view of the radar beam at a 5° tilt angle. The results are shown in Table 2-2.

The tower required to mount the antenna will be a low profile tower with 3.66 m sections with a maximum height of 12.8 m (model LPT1242 from Force 12, Inc.) made of high quality aluminum square tubing with incorporate delrin slides for smooth operation, aircraft quality cables and commercial grade pulleys for some convenience like easy installation and fast up and down movements. Adding the maximum height of the antenna to the transceiver and physical antenna height, the beam exit will be at 14.02 m. Therefore, the calculations of the tilt angles required to have a radar beam obstruction free view were estimated using the previous equations and are displayed in Table 2.2.

Table 2-2
Minimum obstruction free view angles

Obstruction Description (Legend)	$H_{\min}(\text{m})$ for $\theta_{\min}=5^\circ$	$\theta_{\min}(\text{deg})$ $H=3.66 \text{ m}$	$\theta_{\min}(\text{deg})$ $12.8 \text{ m Tower, } H=14.02 \text{ m}$
Tree (1)	15.11	17.5°	6.23°
Tree (2)	13.15	13.8°	4.17°
Tree Line (3)	14.48	12.2°	5.31°
Tree (4)	18.45	13.5°	7.35°
Tree (5)	7.83	7.0°	2.01°
Tree (6)	6.03	6.1°	1.25°
Utility Pole (7)	7.56	13.7°	-9.69°

For comparison purposes, the tilt angles needed to surpass the obstructions at a height of 3.66 m are also included in the table and it can be seen that they decrease considerably with the installation of the antenna on the 12.8 m tower. To get a better visualization of what will happen with the installation of the tower, Figure 2-2 is plotted again in Figure 2-3 with the original measured data (solid line) for H at 3.66 m and the simulated data for H at 14.02 m (dashed line).

Figure 2.9 shows that the minimum elevation angle of the obstructive trees and utility pole is reduced to values below the background clutter. This distant clutter limits the minimum elevation angle to approximately 5° , therefore some obstructions are still over 5° , but they only block 20° of the entire 360° space and must be accepted.

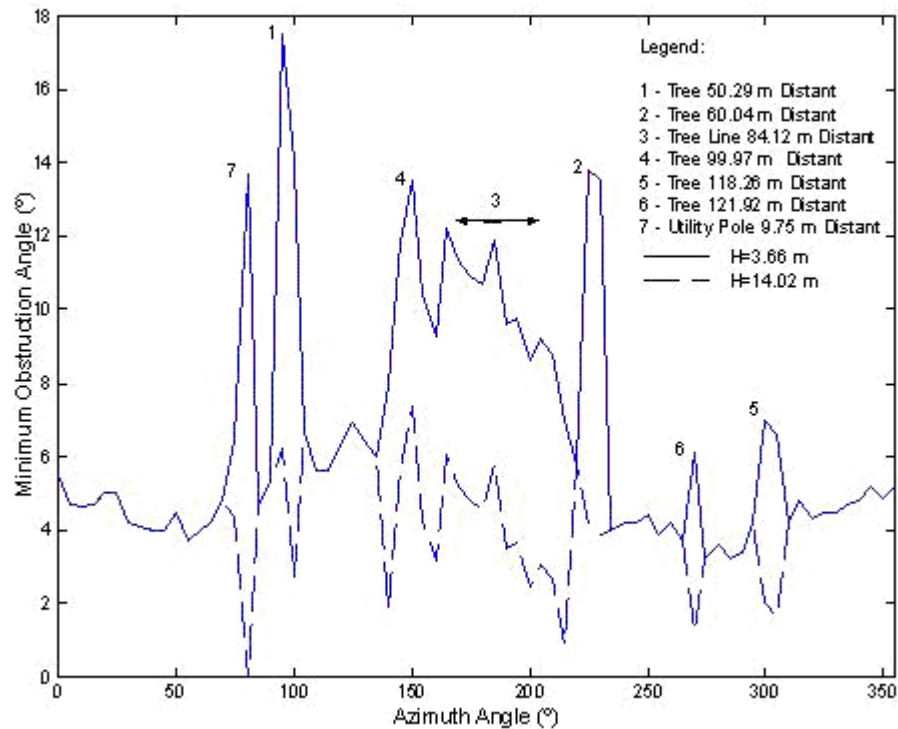


Figure 2.9. Tilson Survey Data Plots (H=3.66 m and H=14.02 m)

The same survey method was implemented in the eleven campuses of the University of Puerto Rico, which is the subject of the next chapter.

CHAPTER 3

RADAR NETWORK SITE SURVEY

3.1 Introduction

Since Puerto Rico is in a tropical environment at the Caribbean, many atmospheric phenomena occur all year round, including hurricanes, tropical storms, heavy rain, etc. The weather forecast of the Island depends on the NEXRAD radar located in a 30 m tower, at the top of a mountain 851 m in height. The radar has a range of 200 Km in a 360° swath. A substantial amount of atmospheric events occur or evolve at the lower part of the troposphere, which is below a height of 1 Km. Also the Earth has a curvature impeding or hiding the lower scatters from the radar footprint at far distances as discussed in Chapter 2. In the case of long-range radars such as NEXRAD information is lost from lower scatters. To resolve that problem, more radars with shorter ranges and located at lower heights should be installed in a network.

In Puerto Rico, the interest is to design and implement a radar network composed of radars located at a short distance (less than 30 Km) between each other. The radars will work in the X-band (9.41 GHz) to obtain a better resolution since the resolution increases with frequency. They will also be polarimetric and will be capable to measure Doppler frequency to obtain information about precipitation rates and particle microstructure.

To implement a test bed in Puerto Rico, a geological survey in some strategic points around the island was made in order to decide the locations for the installation of the antennas. For the survey, the eleven campuses of the University of Puerto Rico were chosen due to accessibility, since the University internet facilities can be used to manage data, electric power is also available and easier maintenance and security exists, among other advantages [9]. The campuses are also evenly distributed around

the island, which makes easier the implementation. In addition, other locations on top of mountains will be studied digitally in order to resolve blind spots and achieve a complete coverage of the Island.

The site survey for the Puerto Rico deployable radar network design is the subject of the chapter.

3.2 Survey procedure and materials

The University of Puerto Rico is comprised of eleven campuses. The campuses are located in Aguadilla, Arecibo, Bayamón, Carolina, Cayey, Humacao, Mayagüez, Ponce, Utuado and two in San Juan (Medical Sciences and Río Piedras campus). With the University of Puerto Rico's eleven campuses as the place where the survey would take place, the first step was to obtain the legal permit to access the campuses. With the legal permits at hand, each campus was surveyed with basically the same method described in Chapter 2.

For the survey, the tallest accessible building of each campus was chosen. In each assessment, the minimum elevation angle to surpass any obstacle was measured in a complete 360° swath. As mentioned in Chapter 2, a distance range meter was used as a telescope to see the obstacles, a digital level measures the inclination angle of the distance range meter, which marks the minimum elevation angle to go beyond the obstacles, and a compass was also used in the survey experiment. Moreover, a Global Positioning System (GPS) receiver was used to get the geographic coordinates in each surveyed point to use as a reference in digital localization. The geographic coordinates are tabulated for each campus in Appendix B.

The minimum elevation or tilt angle that the antennas should have to surpass the obstacles and the minimum antenna height needed to go beyond the nearest obstructions will be calculated using the data obtained in each surveyed site and the equations derived in Chapter 2.

3.3 Survey results and discussion

Each of the eleven campuses of the University of Puerto Rico was successfully surveyed. The minimum angle to surpass the obstacles in a complete 360° swath was tabulated with the geographic coordinates for each campus in Appendix B. Also, images from the satellites IKONOS and Landsat for each campus are shown in Appendix A, each one with the surveyed location point marked.

Each campus data is analyzed in the next subsections.

3.3.1 Aguadilla Campus

A plot of minimum obstruction angle vs. azimuth angle for Aguadilla campus is shown in Figure 3.1 with a picture of the complete 360° swath site panorama matching the plot. The numbers on the plot refer to the obstacles in the Aguadilla Campus survey. The plot shows that some minimum angles are required to surpass the obstructions at a height of 1.5 m (height of telescope) and a 360° azimuth run.

In the survey, the obstacle that requires the highest elevation angle, which is 4°, is a large tree 60 m away from the survey location. Baseball stadium lights and a water tank far away require an antenna tilt angle of 3.3° and 3.4° respectively. Since the stadium lights are at a long distance, a tall antenna tower is needed to clear them and it is not practical. But an antenna tower should be used to reduce the minimum elevation angle of 4° to a minimum angle of 3.4°.

Using Figure 2.8 and Equation 2.4 with an instrument height of 1.5 m instead of 3.66 m, the height of the tower required to surpass the tree with an antenna tilt angle of 3.4° is 3.63 m, which is an acceptable tower height over a building. So the antenna will be at a height of 3.63 m over the Aguadilla campus library and should have an antenna tilt angle of 3.4°.

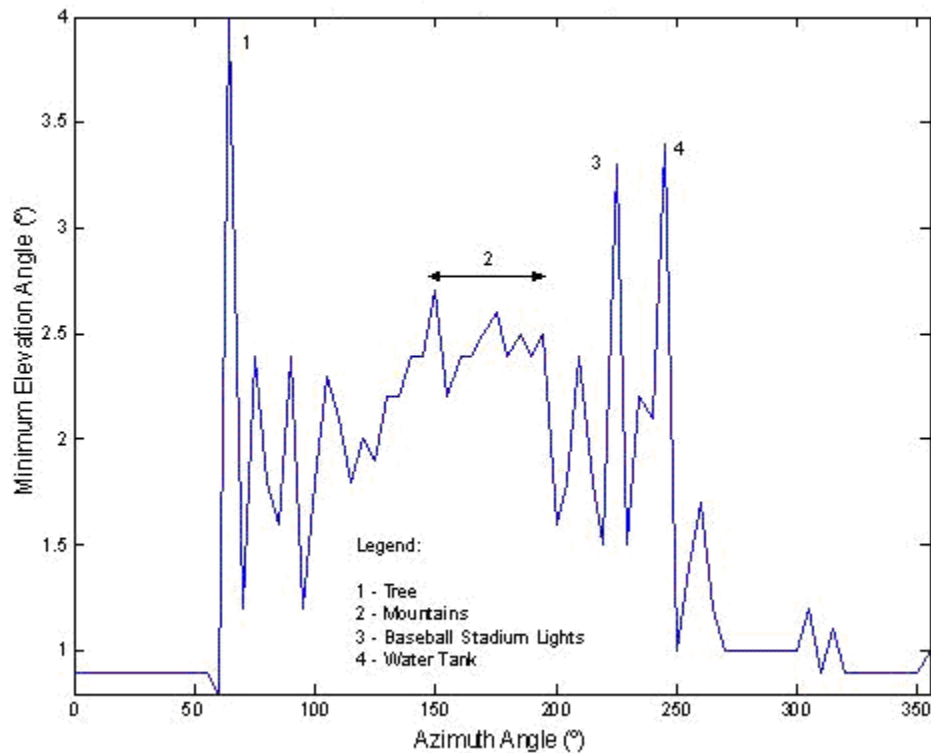


Figure 3.1. Agvadilla campus survey data plot and site panorama

With an antenna inclination angle of 3.4° the radar range can be plotted using Figure 2.2 and Equations 2.2 and 2.3, resulting in Figure 3.2. The plot begins at a vertical height of 85.95 m, which is the total height over sea level including the antenna tower and building heights. The plot is limited up to a height of 5 Km, which is the height where the temperature decreases to approximately 0°C . Also, a point at a height of 1 Km was marked since this is our height for our area of interest. The coverage area up to that height should have a radius of 15.53 Km.

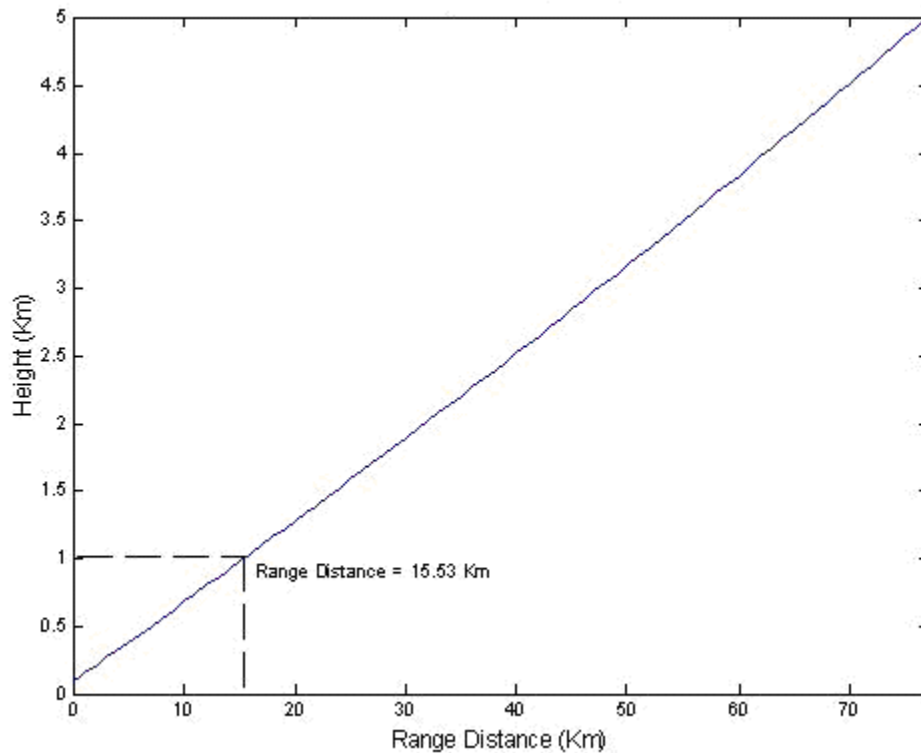


Figure 3.2. Aguadilla campus maximum range plot with a 3.4° tilted beam

3.3.2 Arecibo Campus

A plot of minimum obstruction angle vs. azimuth angle for Arecibo campus is shown in Figure 3.3 with a picture of the complete 360° swath site panorama matching the plot.

From the figure, the obstacle that requires the highest antenna elevation angle, which is 21.8°, is a 5.18 m tower of a microwave antenna located exactly at top of the same building where the survey was made. The tallest electricity pole is located 65.84 m away from the survey point, requiring an antenna tilt angle of 6.6°. Also, the limiting angle is established by the mountains located far away from the point and is 3.3°.

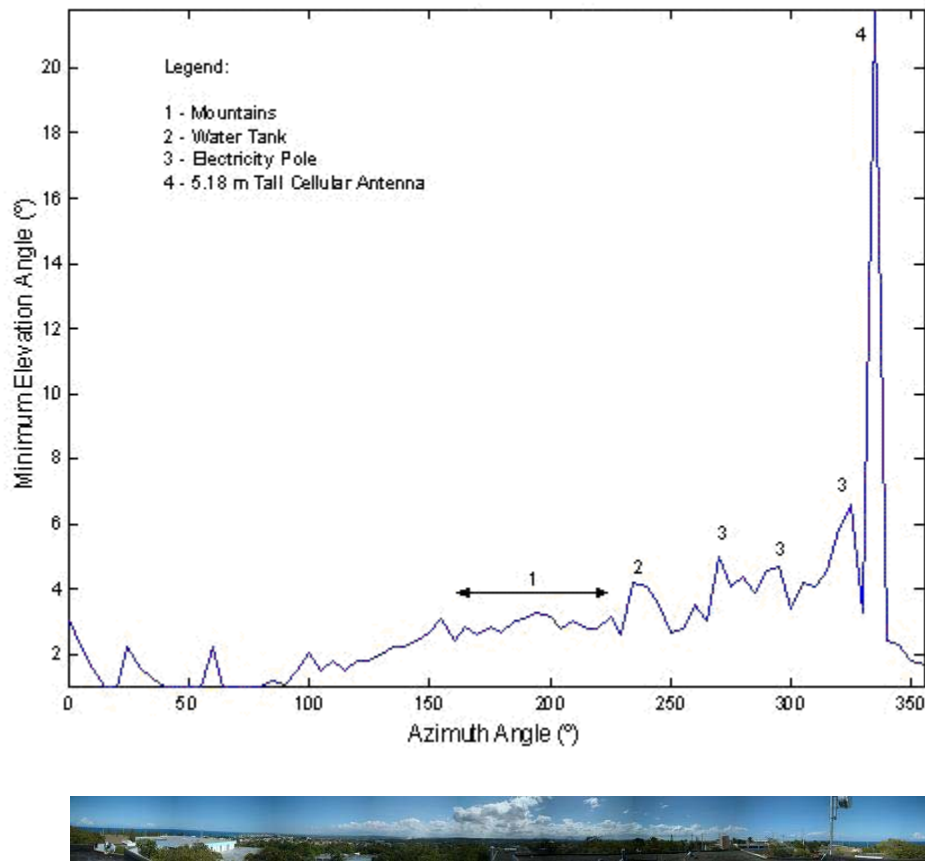


Figure 3.3. Arcibo campus survey data plot and site panorama

Using Figure 2.8 and Equation 2.4 with an instrument height of 1.5 m, the height of the tower required to surpass the electricity pole with an antenna tilt angle of 3.3° is 3.81 m. Since the antenna has to be in a 5.18 meter tower to surpass the microwave antenna tower, all of the nearest obstacles (water tank and electricity poles) must be cleared too. Therefore, the antenna will be at a height of 5.18 m over the Arcibo campus Department of Humanities building and should have an antenna tilt angle of 3.3° , which is limited by the mountains.

With an antenna inclination angle of 3.3° , the radar range can be plotted using Figure 2.2 and Equations 2.2 and 2.3, resulting in Figure 3.4. The plot begins at a vertical height of 70.1 m, which is the total height over sea level including the

antenna tower and building heights. The plot shows that at a height of 1 Km, the radar should only have a range of 15.79 Km. This is a short distance because of the high tilt angle established by the far mountains.

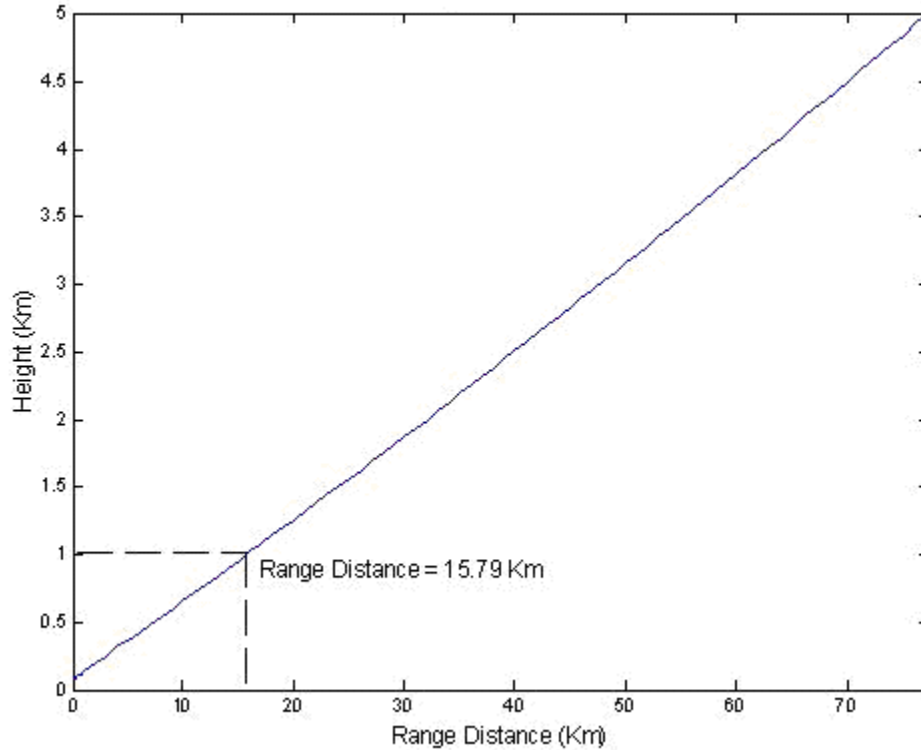


Figure 3.4. Arcibo campus maximum range plot with a 3.3° tilted beam

3.3.3 Bayamón campus

A plot of minimum obstruction angle vs. azimuth angle for Bayamón campus is shown in Figure 3.5 with a picture of the complete 360° swath site panorama matching the plot.

From the figure, the obstacle that requires the highest elevation angle, which is 5°, is a tall mountain located far away from the surveyed location. An extremely tall

antenna tower will be required to reduce the antenna tilt angle and it is not acceptable over the building. So the antenna should have a tilt angle of 5° and will be mounted over a 1.5 m tower.

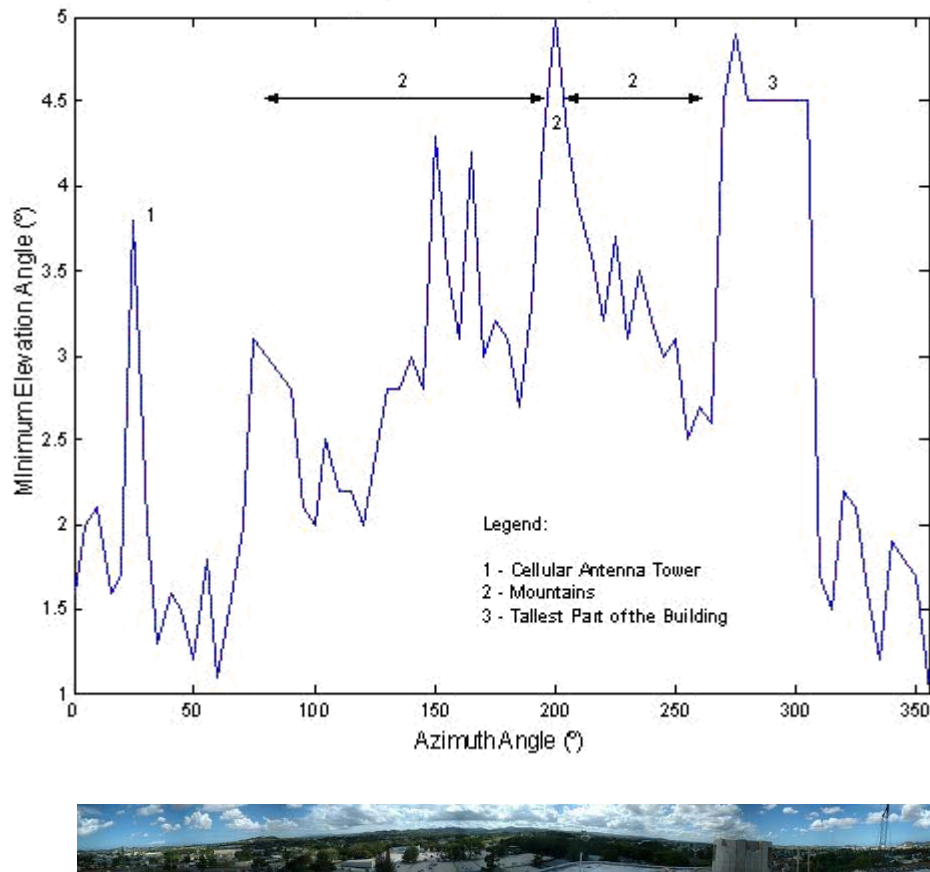


Figure 3.5. Bayamón campus survey data plot and site panorama

With an antenna inclination angle of 5° , the radar range can be plotted using Figure 2.2 and Equations 2.2 and 2.3, resulting in Figure 3.6. The plot begins at a vertical height of 66.75 m, which is the total height over sea level including the antenna tower and building heights. The plot shows that at a height of 1 Km the radar should only have a range of 15.79 Km. This is a short distance because of the high tilt angle established by the far mountains.

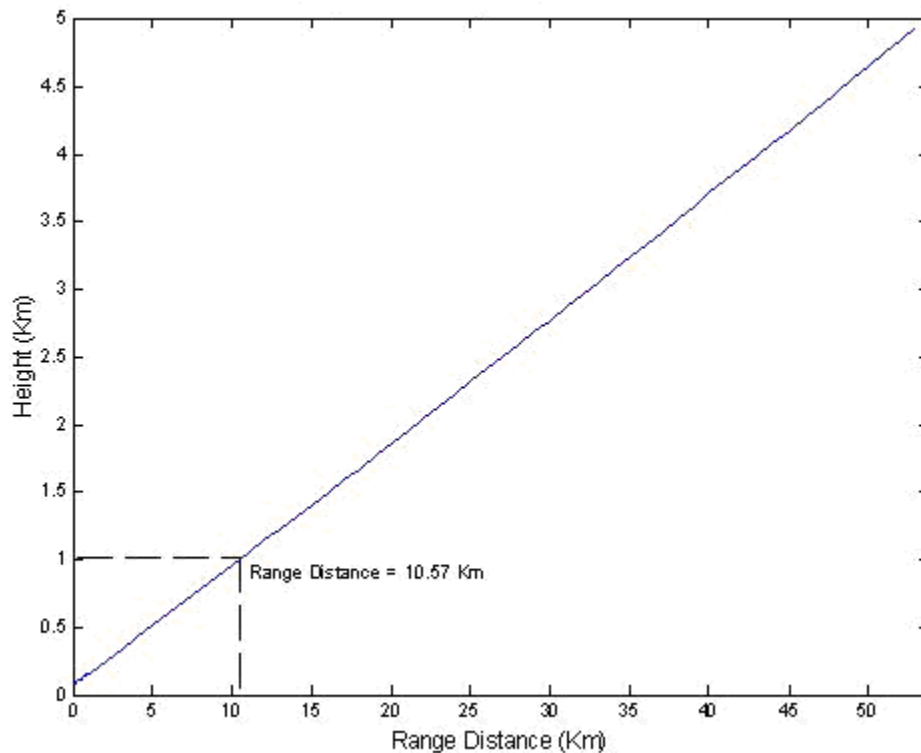


Figure 3.6. Bayamón campus maximum range plot with a 5° tilted beam

3.3.4 Carolina campus

A plot of minimum obstruction angle vs. azimuth angle for Carolina campus is shown in Figure 3.7 with a picture of the complete 360° swath site panorama matching the plot.

From the figure, the obstacle that requires the highest elevation angle, which is 14.1°, is a tall mountain located 610 m away from the surveyed location. Using Figure 2.8 and Equation 2.4 with an instrument height of 1.5 m, the height of the tower required to surpass the mountain with an antenna tilt angle of 3.2° is 119.12 m. Since the antenna has to be on a 119.12 m tower to surpass the mountain, all of the

nearest obstacles (pines and trees) must be cleared too. So an extremely tall tower will be required to reduce the antenna tilt angle and this is not acceptable.

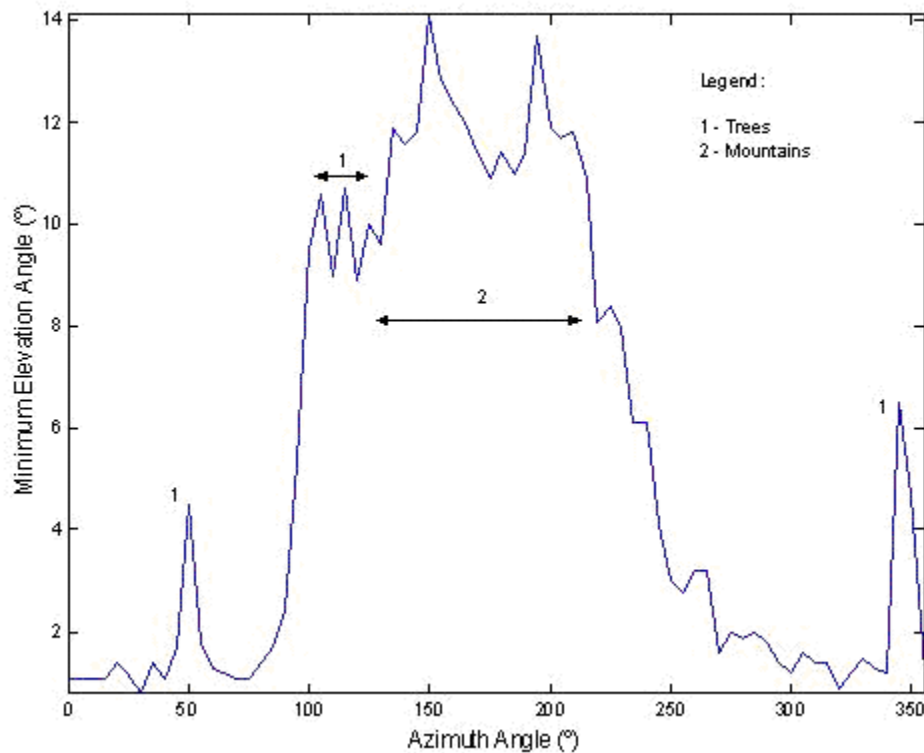


Figure 3.7. Carolina campus survey data plot and site panorama

With an antenna inclination angle of 14.1° , the radar range can be plotted using Figure 2.2 and Equations 2.2 and 2.3, resulting in Figure 3.8. The plot begins at a vertical height of 63.09 m, which is the total height over sea level including the height of the building. The plot shows that at a height of 1 Km the radar should only have a range of 3.73 Km, which is a short distance because of the high tilt angle established by the mountain. That tilt angle is not acceptable to install an antenna; hence Carolina campus will not be used as a node for the radar network.

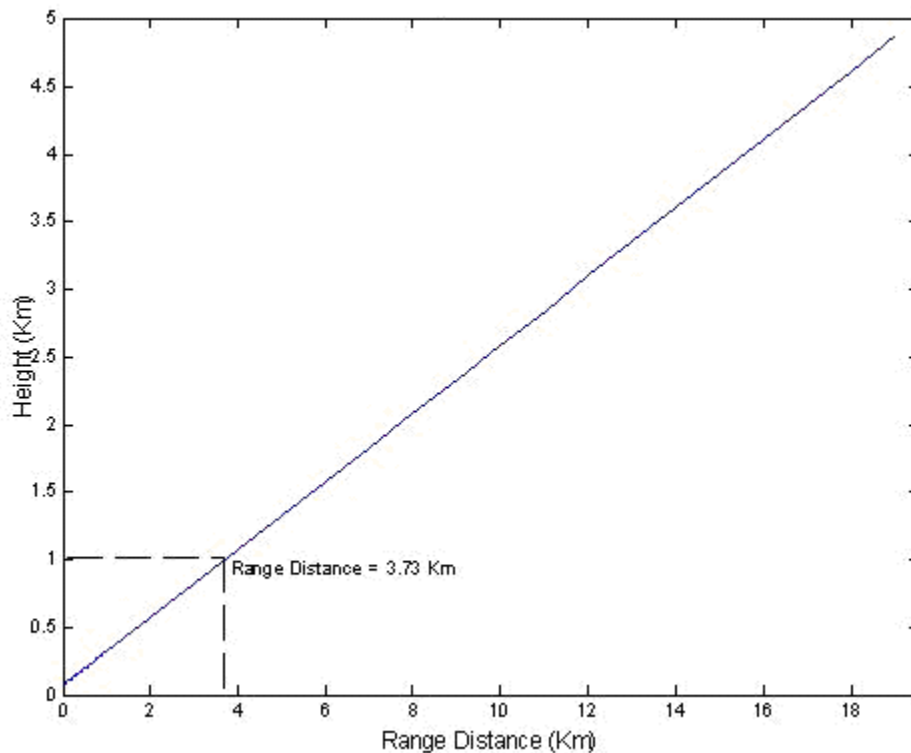


Figure 3.8. Carolina campus maximum range plot with a 14.1° tilted beam

3.3.5 Cayey campus

A plot of minimum obstruction angle vs. azimuth angle for Cayey campus is shown in Figure 3.9 with a picture of the complete 360° swath site panorama matching the plot.

From the figure, the obstacle that requires the highest antenna elevation angle, which is 18° , is a 6.6 m pine tree located exactly behind the building where the survey was made. In addition a big tree line requiring a maximum antenna tilt angle of 16° is located 540 m away from the survey point. The limiting angle established by the mountains is 8.8° .

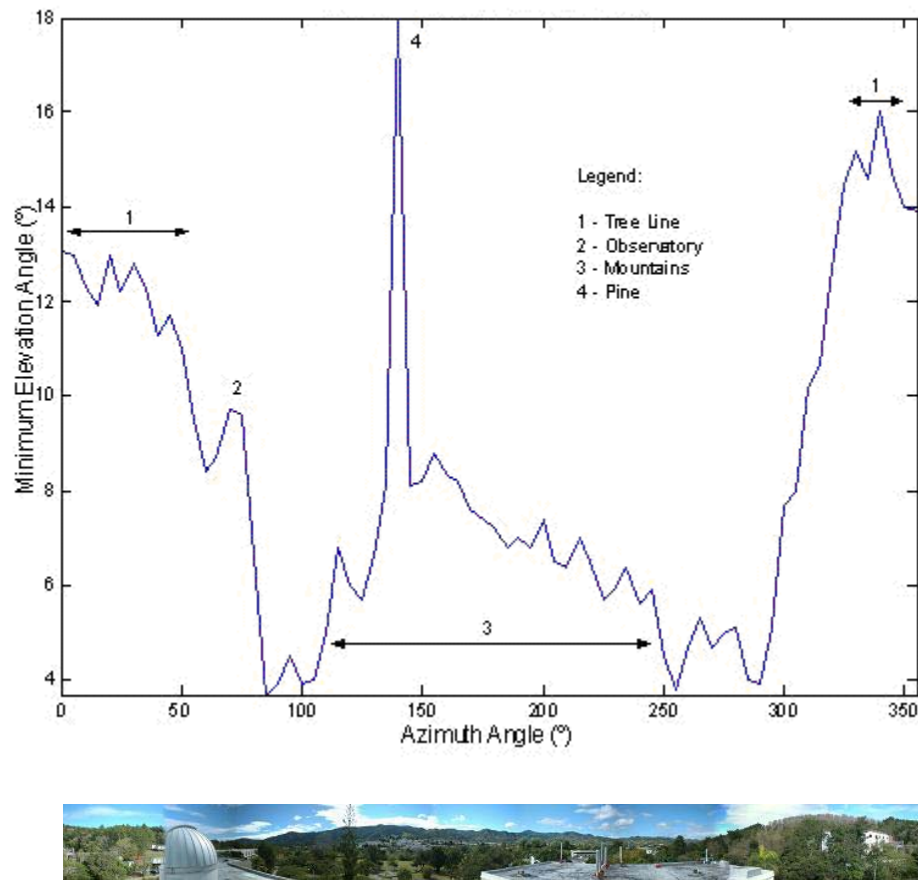


Figure 3.9. Cayey campus survey data plot and site panorama

Using Figure 2.8 and Equation 2.4 with an instrument height of 1.5 m, the height of the tower required to surpass the tree line with an antenna tilt angle of 8.8° is 70.4 m. An antenna tower height of 70.4 m is not acceptable on top of the building. In addition, with the 8.8° antenna tilt angle established by the mountain, the range of the radar will be very small and will not be cost effective.

With an antenna inclination angle of 16° , the radar range can be plotted using Figure 2.2 and Equations 2.2 and 2.3, resulting in Figure 3.10. The plot begins at a vertical height of 421.84 m, which is the total height over sea level including the height of the building. The plot shows that at a height of 1 Km the radar should only have a range of 2.02 Km, which is a short distance because of the high tilt angle

established by the tree line. That tilt angle is not acceptable to install an antenna; hence Cayey campus will be rejected as a node for the radar network as well.

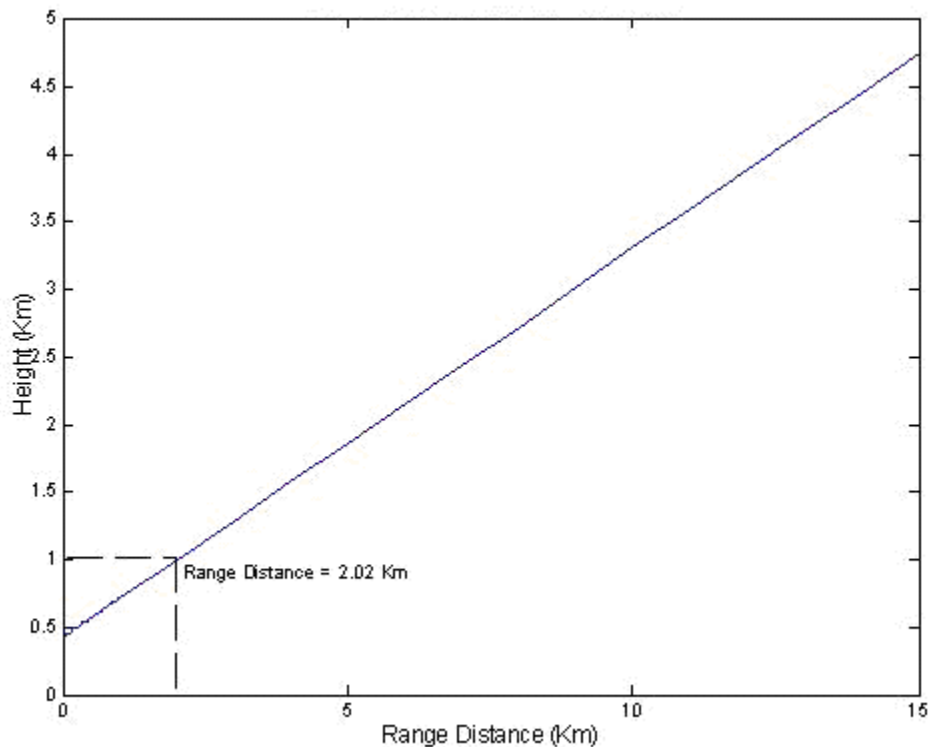


Figure 3.10. Cayey campus maximum range plot with a 16° tilted beam

3.3.6. Humacao campus

A plot of minimum obstruction angle vs. azimuth angle for Bayamón campus is shown in Figure 3.11 with a picture of the complete 360° swath site panorama matching the plot.

From the figure, the obstacle that requires the highest antenna vertical angle, which is 6°, is a tall mountain located far away from the surveyed location. A tall antenna tower will be required to reduce the antenna tilt angle and this is not

acceptable on top of the building. Therefore, the antenna should have a tilt angle of 6° and will be mounted at the top of the library building.

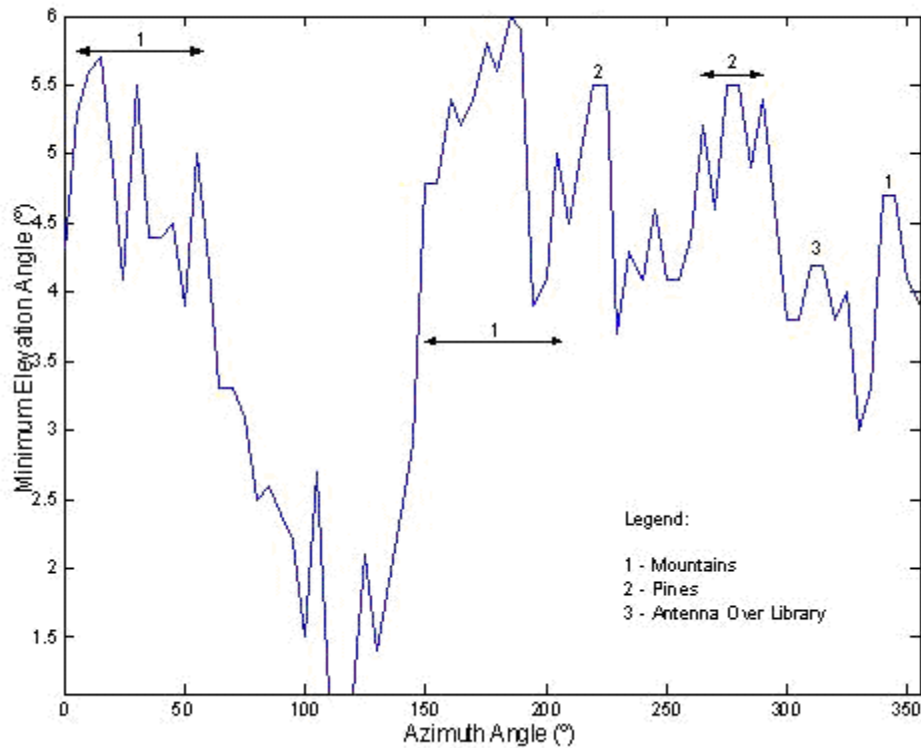


Figure 3.11. Humacao campus survey data plot and site panorama

With an antenna inclination angle of 6° , the radar range can be plotted using Figure 2.2 and Equations 2.2 and 2.3, resulting in Figure 3.12. The plot begins at a vertical height of 53.95 m, which is the total height over sea level including the building height. The plot shows that at a height of 1 Km the radar should only have a range of 8.94 Km, which is a short distance because of the high tilt angle established by the far mountains.

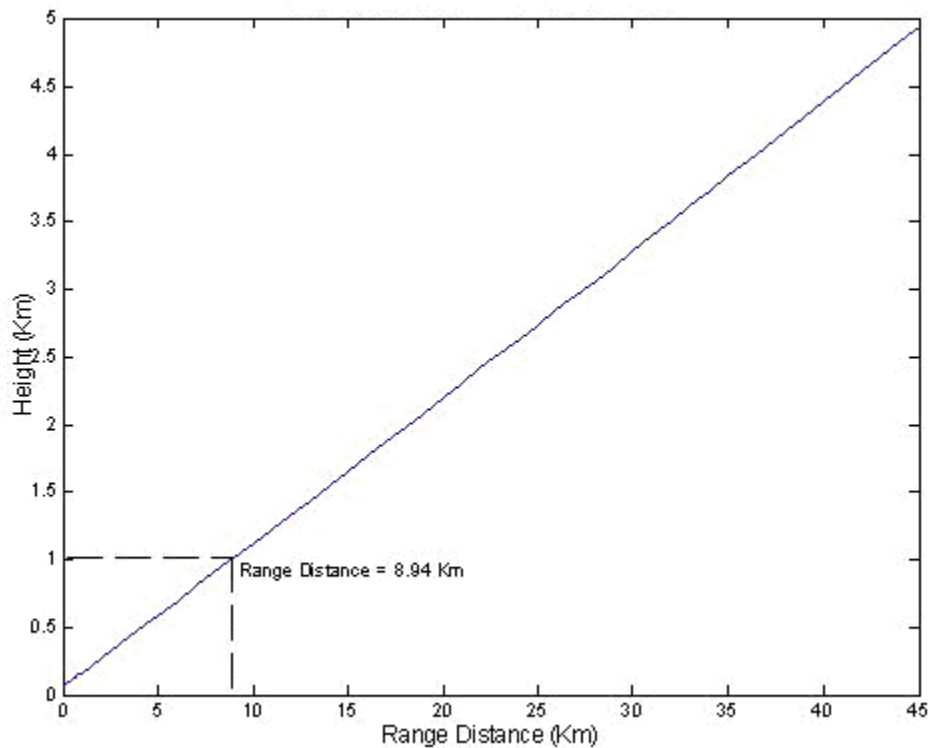


Figure 3.12. Humacao campus maximum range plot with a 6° tilted beam

3.3.7 Mayagüez campus

A plot of minimum obstruction angle vs. azimuth angle for Mayagüez campus is shown in Figure 3.13 with the corresponding picture of the complete 360° swath site panorama matching the plot.

From the figure, a tall mountain located far away is the obstacle that requires the highest antenna vertical angle, which is 4.8°. A tall antenna tower will be required to reduce the antenna tilt angle and this is not acceptable on top of the building. Therefore, the antenna should have a tilt angle of 4.8° and will be mounted at the top of the chemistry building.

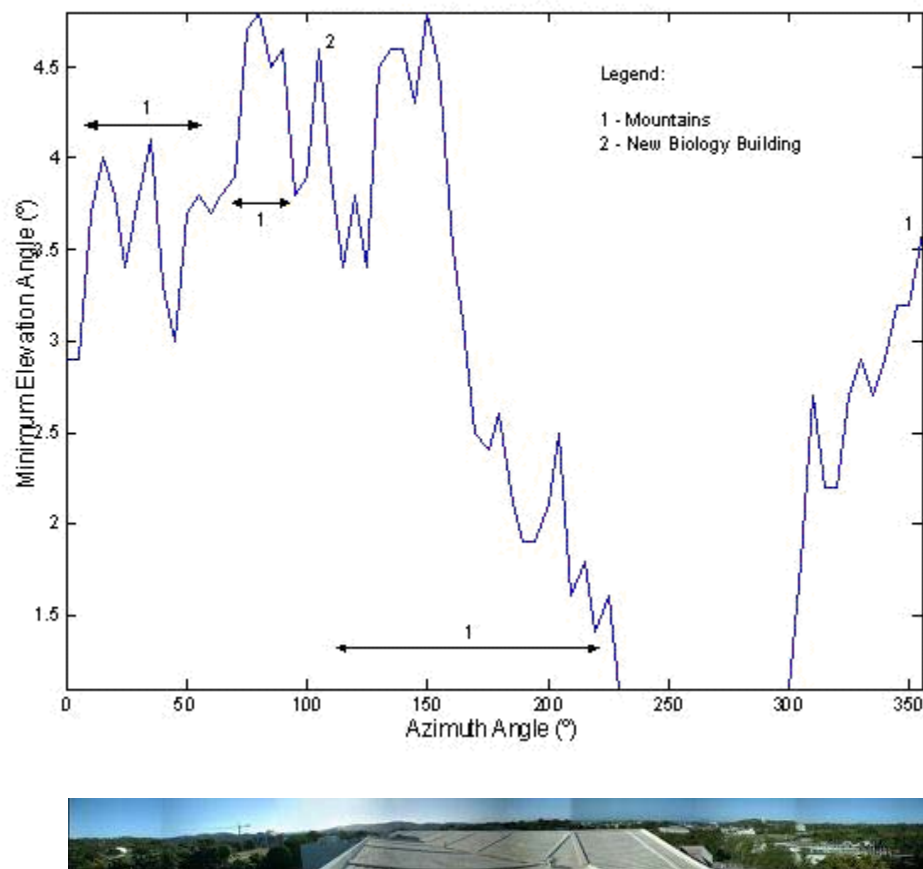


Figure 3.13. Mayagüez campus survey data plot and site panorama

With an antenna inclination angle of 4.8° , the radar range can be plotted using Figure 2.2 and Equations 2.2 and 2.3, resulting in Figure 3.14. The plot begins at a vertical height of 52.12 m, which is the total height over sea level including the building height. The plot shows that at a height of 1 Km the radar should have only a range of 11.17 Km, which is a short distance because of the high tilt angle established by the far mountains.

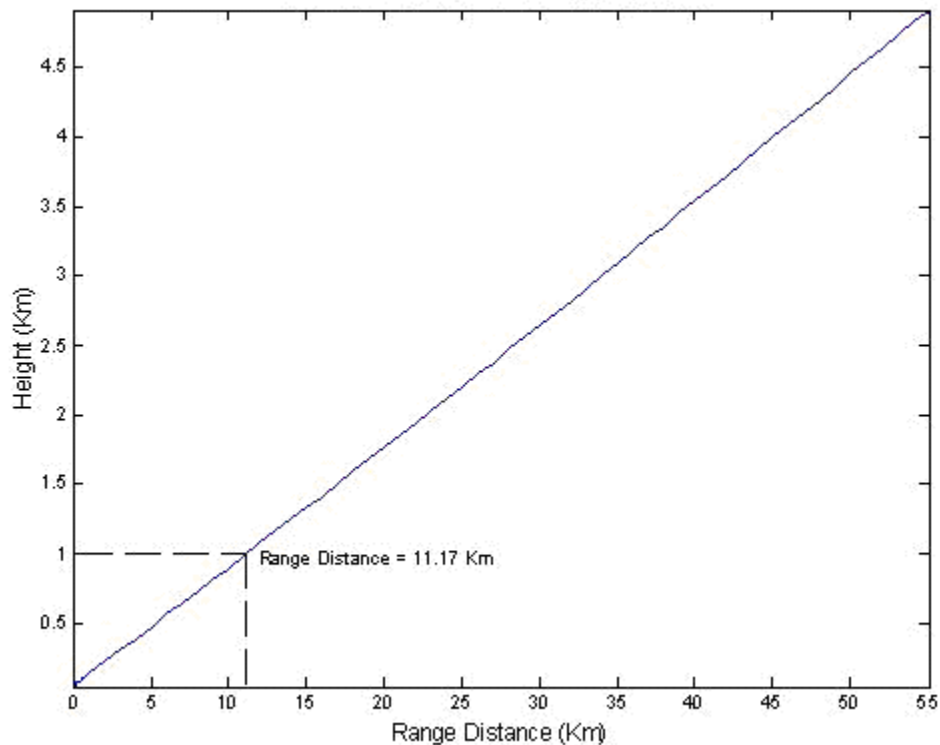


Figure 3.14. Mayagüez campus maximum range plot with a 4.8° tilted beam

3.3.8 Medical Sciences campus

A plot of minimum obstruction angle vs. azimuth angle for Medical Sciences campus is shown in Figure 3.15 with the corresponding picture of the complete 360° swath site panorama matching the plot.

From the figure, the tallest obstacle is a 7.62 m radio frequency antenna located exactly on top of the building. In addition, three groups of pipes are located at the side of the building, requiring antenna tilt angles of 7.8°, 8.6° and 8°, respectively. The groups of pipes are located at 30.48 m, 15.24 m, and 32.61 m away from the surveyed point location. To surpass the mountains, an antenna tilt angle of 3.5° is required.

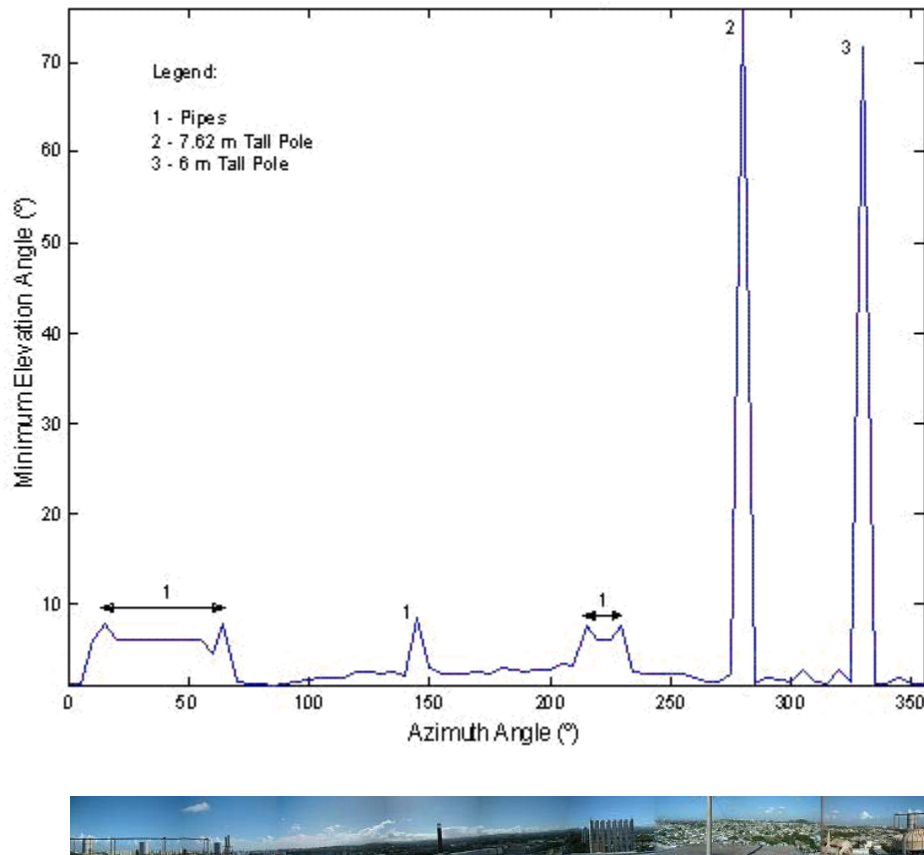


Figure 3.15. Medical Sciences campus survey data plot and site panorama

Using Figure 2.8 and Equation 2.4 with an instrument height of 1.5 m, the height of the tower required to surpass the groups of pipes with an antenna tilt angle of 3.5° is 4.2 m. Since the height of the tower required to surpass the radio frequency antenna is 7.62 m, the groups of pipes will be cleared too. In this campus, the radar antenna will be at a height of 7.62 m with a tilt angle of 3.5° .

Using Figure 2.2 and Equations 2.2 and 2.3 with an antenna tilt angle of 3.5° , the radar range can be plotted resulting in Figure 3.16. The plot begins at a vertical height of 72.54 m, which is the total height over sea level including the building height and antenna height. The plot shows that at a height of 1 Km the radar should

only have a range of 14.88 Km, which is a short distance because of the high tilt angle established by the far mountains.

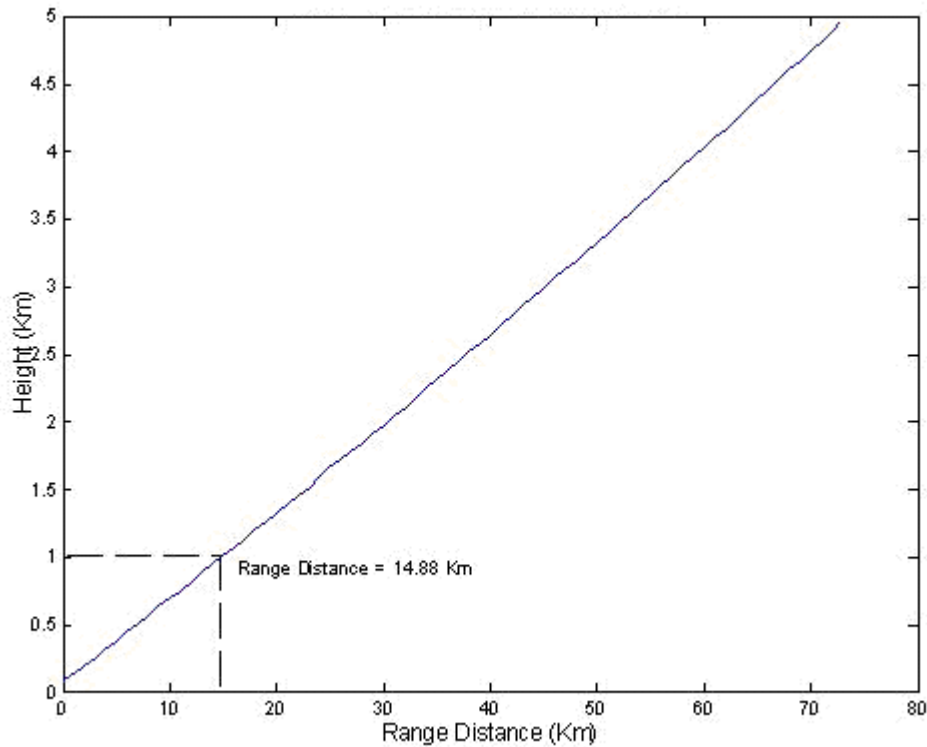


Figure 3.16. Medical Sciences campus maximum range plot with a 3.5° tilted beam

3.3.9 Ponce Campus

A plot of minimum obstruction angle vs. azimuth angle for Ponce campus is shown in Figure 3.17 with the corresponding picture of the complete 360° swath site panorama matching the plot.

From the figure, the tallest obstacle is a 3.05 m tall sign located 8.53 m away from the surveyed location that requires an antenna tilt angle of 7.6°. The Ponce Judicial Center Building is located at a distance of 400 m from the survey location and

requires an antenna elevation angle of 7.4° . Therefore, to surpass the mountains an antenna tilt angle of 5.2° is required.

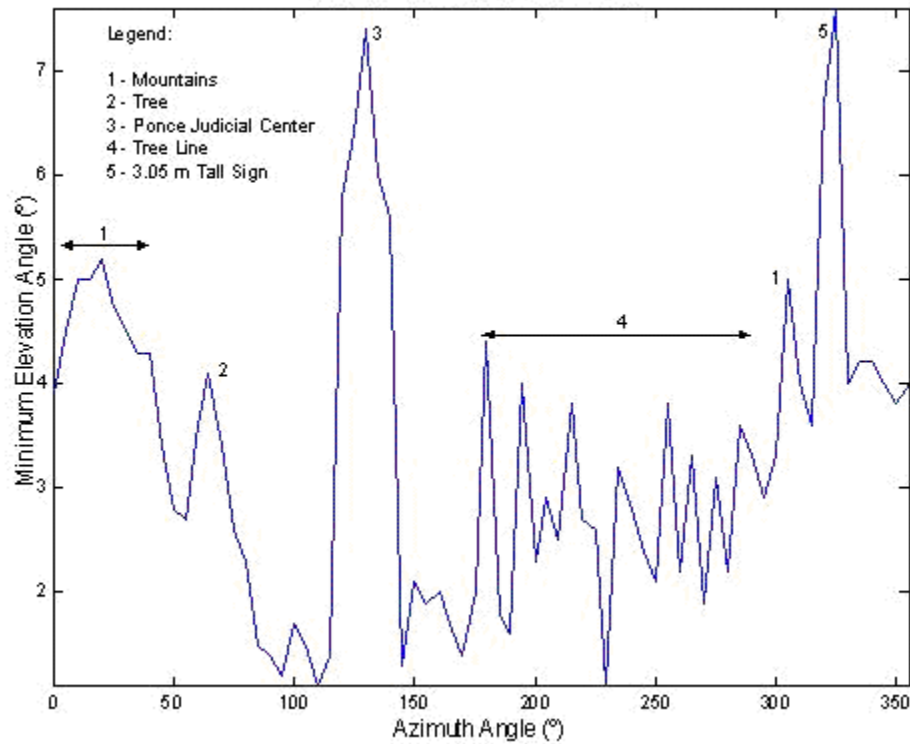


Figure 3.17. Ponce campus survey data plot and site panorama

Using Figure 2.8 and Equation 2.4 with an instrument height of 1.5 m, the height of the tower required to surpass the Ponce Judicial Center building with an antenna tilt angle of 5.2° is 17.05 m. Since the height of the tower required to surpass the Ponce Judicial Center building is 17.05 m, the sign will be cleared too. In this campus, the radar antenna will be at a height of 17.05 m over the building with a tilt angle of 5.2° .

Using Figure 2.2 and Equations 2.2 and 2.3 with an antenna tilt angle of 5.2° , the radar range can be plotted resulting in Figure 3.18. The plot begins at a vertical

height of 31.09 m, which is the total height over sea level including the building height and antenna height. The plot shows that at a height of 1 Km the radar should only have a range of 10.66 Km, which is a short distance because of the high tilt angle established by the far mountains.

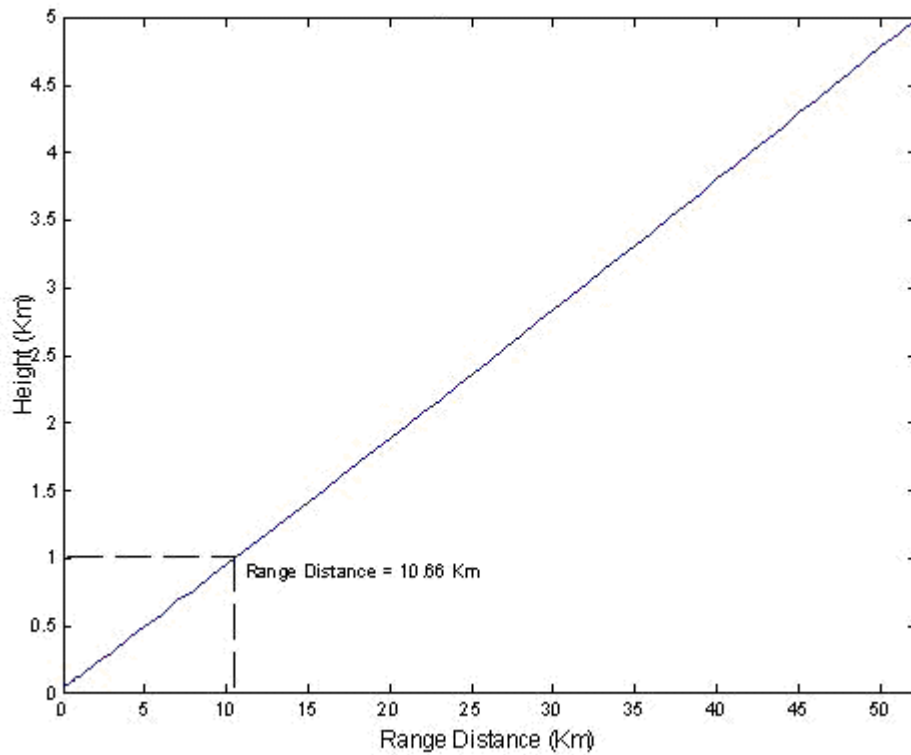


Figure 3.18. Ponce campus maximum range plot with a 5.2° tilted beam

3.3.10 Río Piedras campus

A plot of minimum obstruction angle vs. azimuth angle for Río Piedras campus is shown in Figure 3.19 with the corresponding picture of the complete 360° swath site panorama matching the plot.

From the figure, the tallest obstacle is a 4.57 m tall T.V. antenna located exactly on top of the North Tower building requiring an antenna tilt angle of 32° . Another two T.V. antennas and a concrete wall are also located on top of the building, requiring antenna tilt angles of 29° , 24.3° and 8.7° , respectively. Therefore, to surpass the mountains an antenna tilt angle of 3.3° is required.

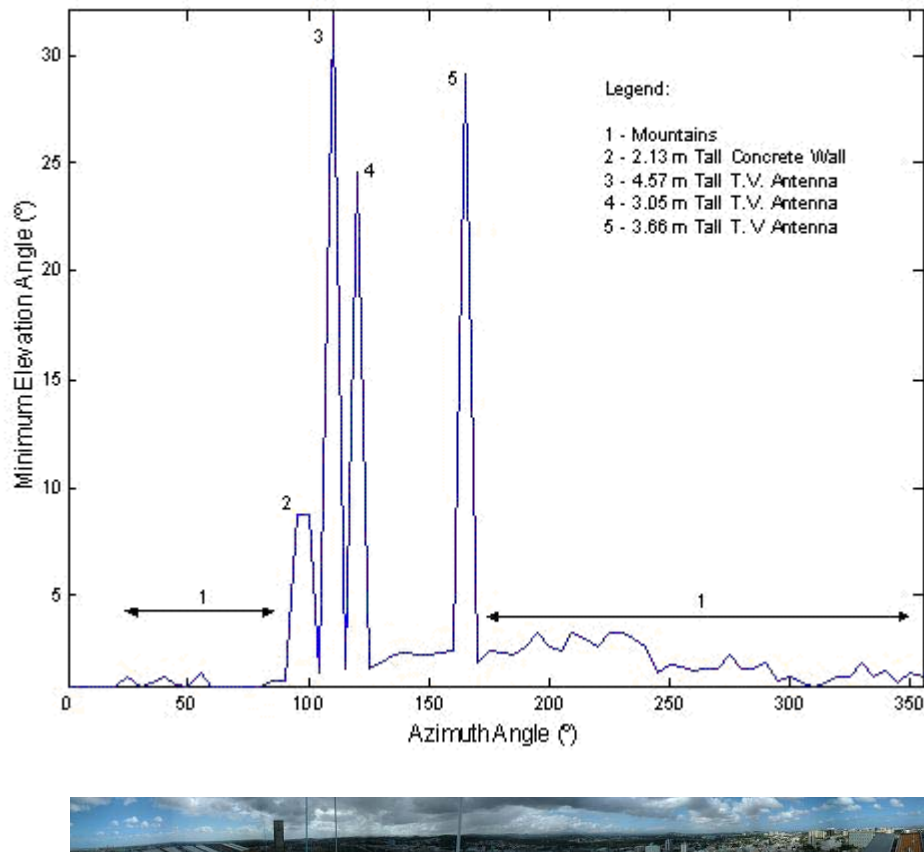


Figure 3.19. Rio Piedras campus survey data plot and site panorama

Using Figure 2.8 and Equation 2.4 with an instrument height of 1.5 m, the height of the tower required to surpass the tallest T.V. antenna is 4.57 m. Since the height of the tower required to surpass the tallest antenna is 4.57 m, the other obstacles will be

cleared too. In this campus, the radar antenna will be at a height of 4.57 m over the building with a tilt angle of 3.3° .

Using Figure 2.2 and Equations 2.2 and 2.3 with an antenna tilt angle of 3.3° , the radar range can be plotted resulting in Figure 3.20. The plot begins at a vertical height of 89.92 m, which is the total height over sea level including the building height and antenna height. The plot shows that at a height of 1 Km the radar should have only a range of 15.46 Km, which is a short distance because of the high tilt angle established by the far mountains.

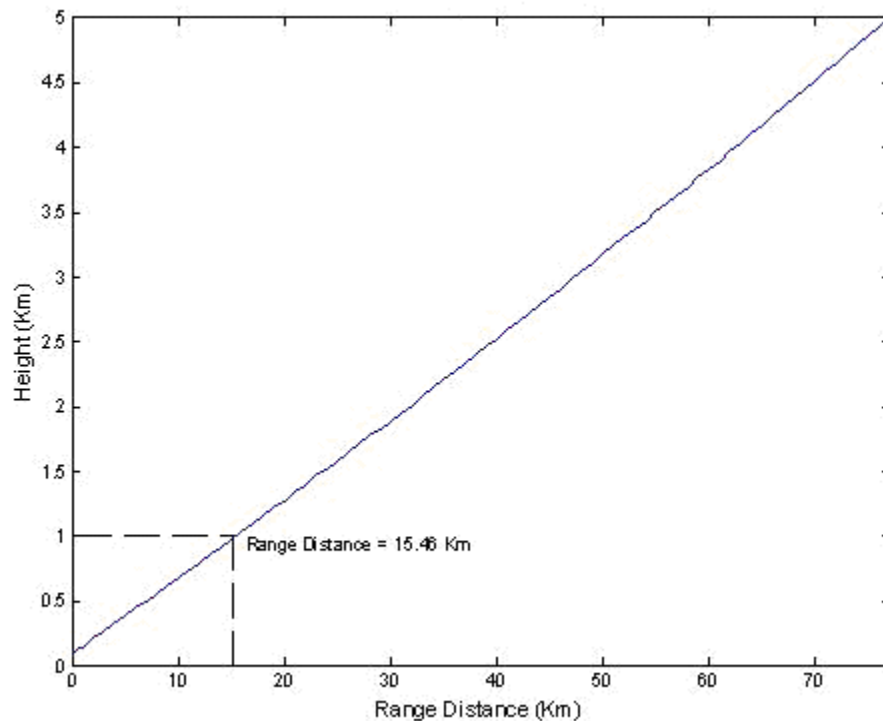


Figure 3.20. Río Piedras campus maximum range plot with a 3.3° tilted beam

3.3.11 Utuado campus

A plot of minimum obstruction angle vs. azimuth angle for Utuado campus is shown in Figure 3.21 with a picture of the complete 360° swath site panorama matching the plot.

From the figure, a tall mountain located far away is the obstacle that requires the bigger antenna vertical angle, which is 11.3°. A tall antenna tower will be required to reduce the antenna tilt angle and this is not acceptable on top of the building. Therefore, the antenna should have a tilt angle of 11.3° and will be mounted on top of Building B. With that antenna tilt angle established by the mountain, the range of the radar will be very small and will not be cost effective.

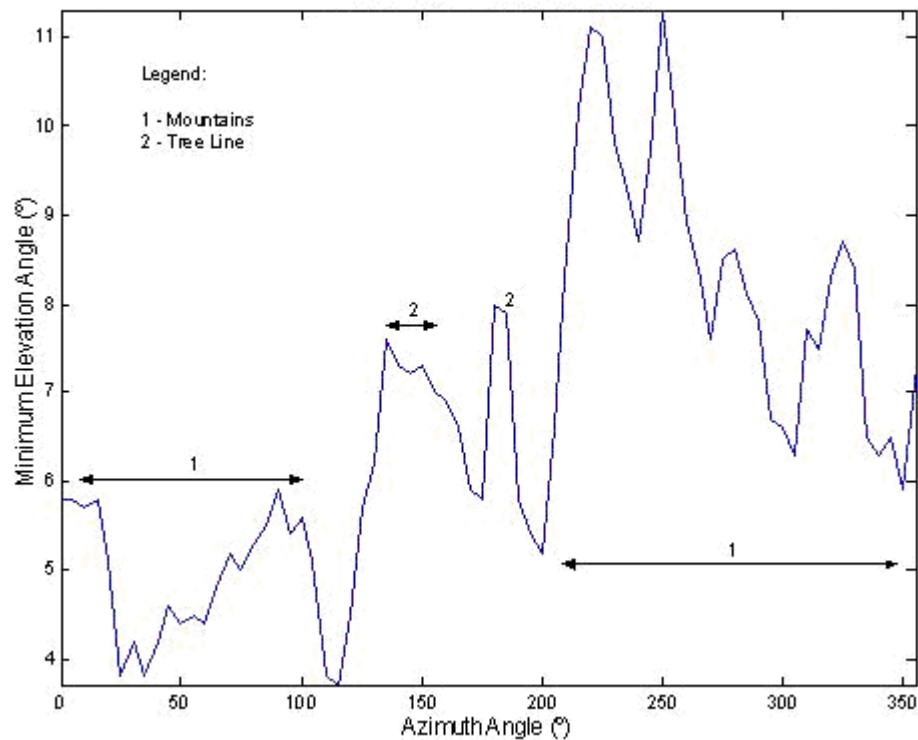


Figure 3.21. Utuado campus survey data plot and site panorama

With an antenna inclination angle of 11.3° the radar range can be plotted using Figure 2.2 and Equations 2.2 and 2.3, resulting in Figure 3.22. The plot begins at a vertical height of 195.98 m, which is the total height over sea level including the height of the building. The plot shows that at a height of 1 Km the radar should only have a range of 4.02 Km, which is a short distance because of the high tilt angle established by the mountains. This tilt angle is not acceptable to install an antenna; hence Cayey campus will not be used as a node for the radar network as well.

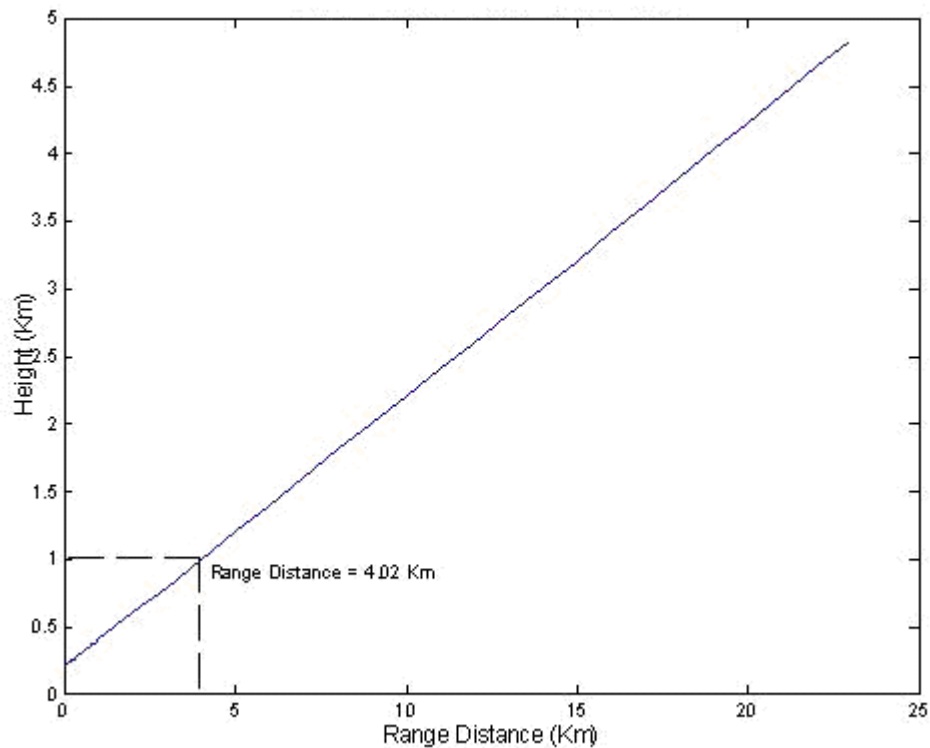


Figure 3.22. Utuado campus maximum range plot with a 11.3° tilted beam

3.4 Radar network coverage

With each surveyed campus point location, antenna inclination angle, antenna height, and maximum radar range defined, each campus coverage can be plotted over a Puerto Rico map using a complete 360° swath circles. Maps using different radar ranges and different node locations over the mountains are used for comparison purposes.

3.4.1 Maximum range definition

As seen in section 3.3, all campus range plots had been limited to a height of 5 Km, which is the height where the temperature decreases to approximately 0°C, hence the water begins to freeze and no more information from precipitation can be obtained. A plot of temperature vs. vertical height with data obtained in March 2003 from a sounding at the area of San Juan, Puerto Rico is shown in Figure 3.23.

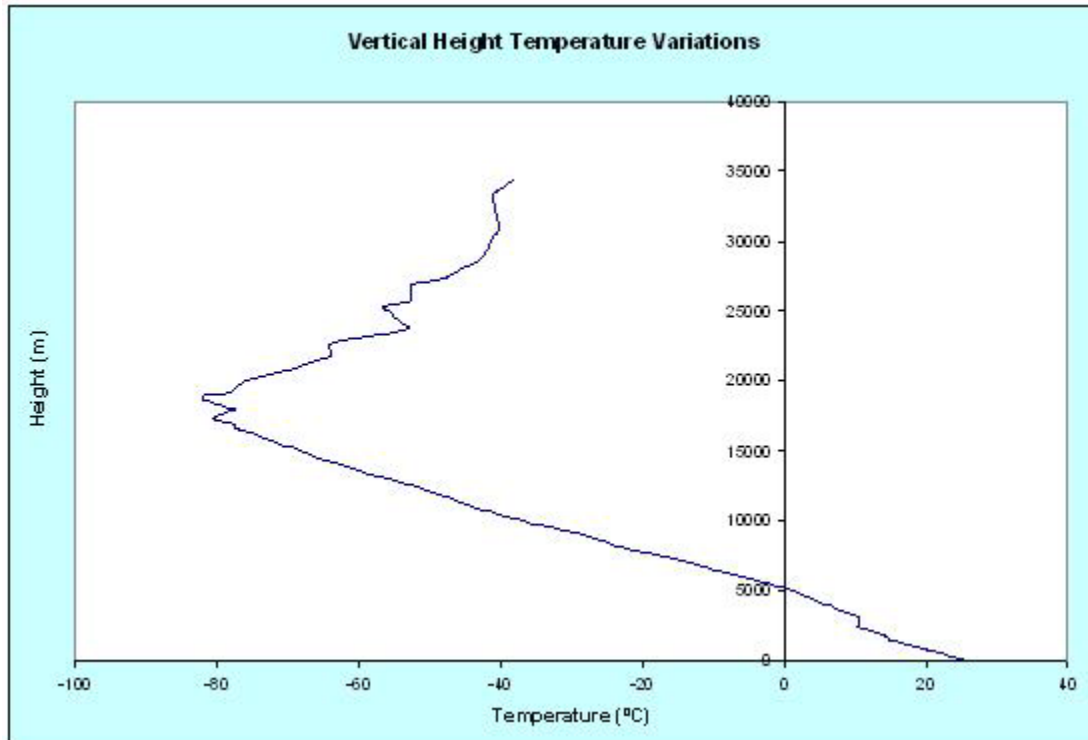


Figure 3.23. Vertical height temperature variations in the San Juan area, obtained on March 2003.

The plot shows that slightly above 5 Km of height, the temperature decreases to 0°C, which is our maximum height to obtain valuable precipitation information. In addition, the curve presents a linear behavior from the beginning of the plot up to 16.5 Km, defining the troposphere up to that point. An equation to model the linear behavior for the troposphere can be obtained using the linear regression tool.

From the beginning of the plot up to 3 Km, the temperature decreases with height at a rate of 6.4°C per Kilometer. Applying the linear regression tool, the equation that models the linear variation of temperature with height up to 3 Km results in

$$T(z) = T_0 - 6.4z, \text{ } ^\circ\text{C} \quad (3.1)$$

where z is the vertical height from the Earth in Km and T_0 is the temperature at the surface of the Earth in °C. Slightly after 3 Km, the temperature stays constant and then begins to decrease linearly again up to 16.5 Km at a rate of 6.9°C. Hence applied the linear regression tool, the equation that models the linear variation of temperature with height up to 16.5 Km results in

$$T(z) = T_0 - 6.9z, \text{ } ^\circ\text{C} \quad (3.2)$$

Equations 3.1 and 3.2 can only be used to model the vertical temperature variations in the area of Puerto Rico, since it depends on the latitude where the measurements were taken. A standard model for the U.S. can be found in Chapter 5 of [10].

3.4.2 Campuses coverage representation

From Figure 3.23 the maximum range that the radar should have was obtained and will be limited to the range where the beam reaches a height of 5 Km. With the antenna tilt angle established in section 3.3 for each campus and with a maximum coverage of each campus up to a height of 4 Km the Island has a complete coverage and Figure 3.24 is obtained.

From the figure, only a range up to 4 Km was used since the Island is completely covered with that range. Carolina, Cayey and Utuado campus were eliminated from the map because of the high antenna elevation angle requirement, which made the nodes not cost effective. Bayamón and Medical Sciences were eliminated from the map as well, because Río Piedras campus covers their area and the use of nodes with less than 20 Km between them will not be cost effective, unless they are used as spare nodes for reliability purposes.

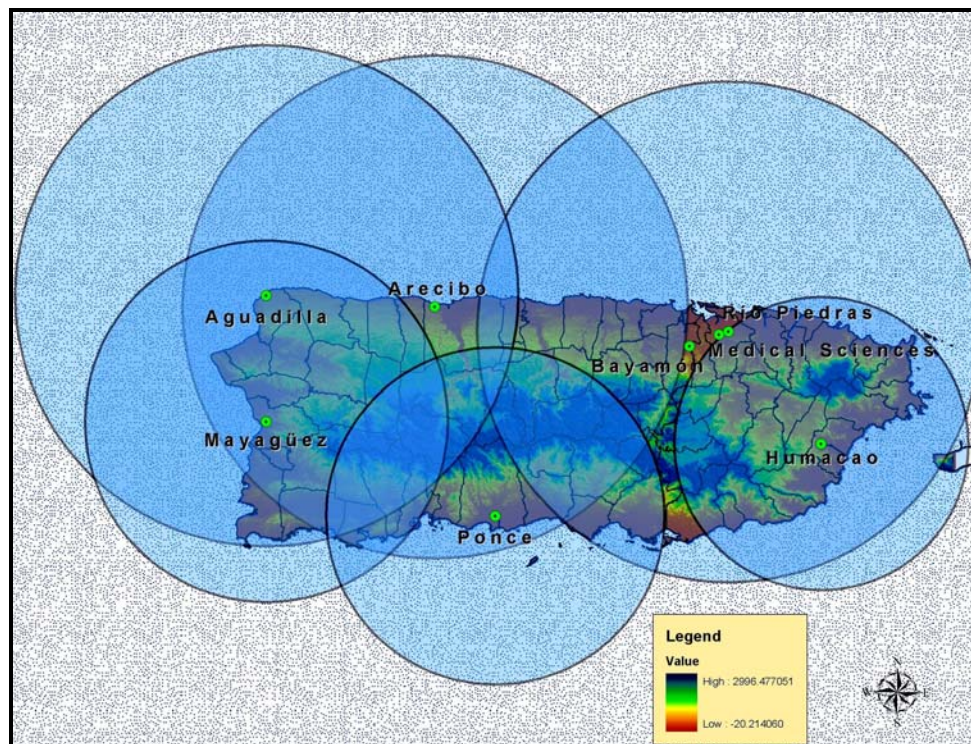


Figure 3.24. Radar network coverage using 4 Km height circles.

It is easy to observe from the coverage map that only using Aguadilla, Arecibo, Humacao, Mayagüez, Ponce and Río Piedras campuses and the complete radar range, the Island will have a complete coverage. But we are interested in studying only the lower part of the atmosphere or below a height of 1 Km.

As mentioned in Chapter 1, the purpose of the radar network is to solve the curved Earth issue using nodes which are close to each other to study the lower part of the troposphere. Subsequently, the area of interest of the total range will be the below 1 Km. Using the same antenna tilt angle defined in section 3.3 for each node and a maximum range established by 1 Km of height, the coverage map is shown in Figure 3.25.

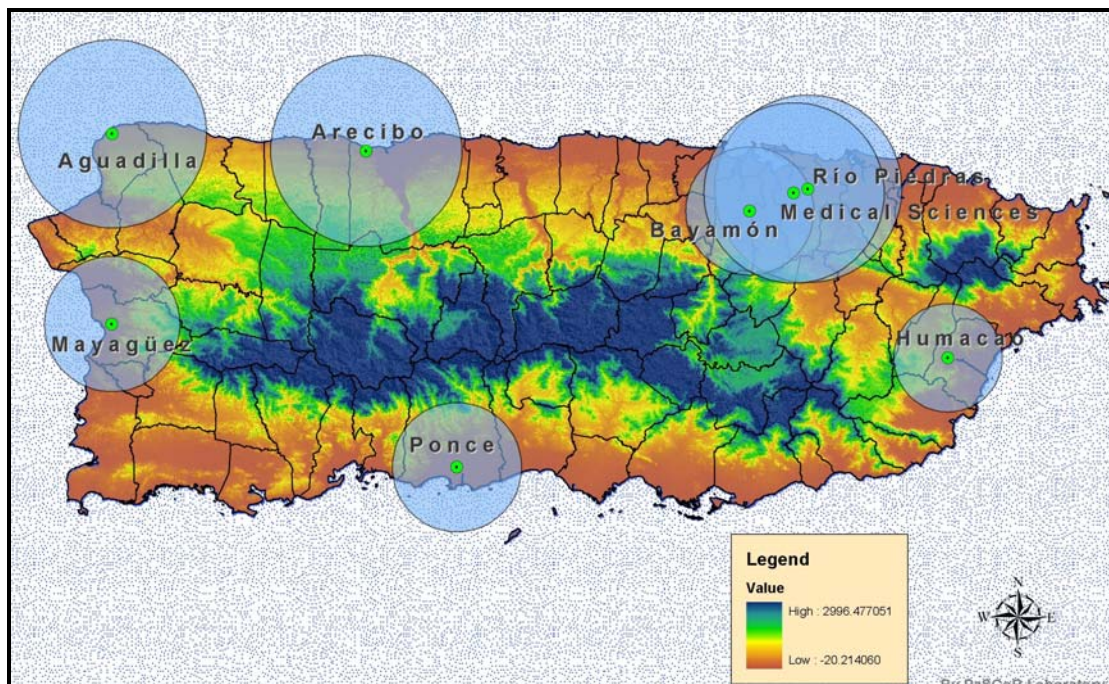


Figure 3.25. Radar network coverage using 1 Km maximum height circles.

The figure shows that up to a height of 1 Km the coverage of the Island will be very small due to the high antenna tilt angle required to surpass the high mountains at

the center of the Island, which indicates that more radars on top of the mountains will be required to have a better or complete coverage of the Island.

Using one node on top of “Monte Guilarte” (18 08 28.20201 N, 66 46 08.60097 W), “Cerro Punta” (18 10 21.79406 N, 66 35 31.81867 W), “Pico El Toro” (18 04 58.17835 N, 65 49 57.11028 W), and one in Cayey (18 06 54.37636 N, 66.04 47.22513 W) with a sea level height of 1.204 Km, 1.338 Km, 1.074 Km, and 851 m respectively, the coverage of the Island will look as in Figure 3.26. They were chosen strategically to cover the island, since they are the highest points in the area of coverage.

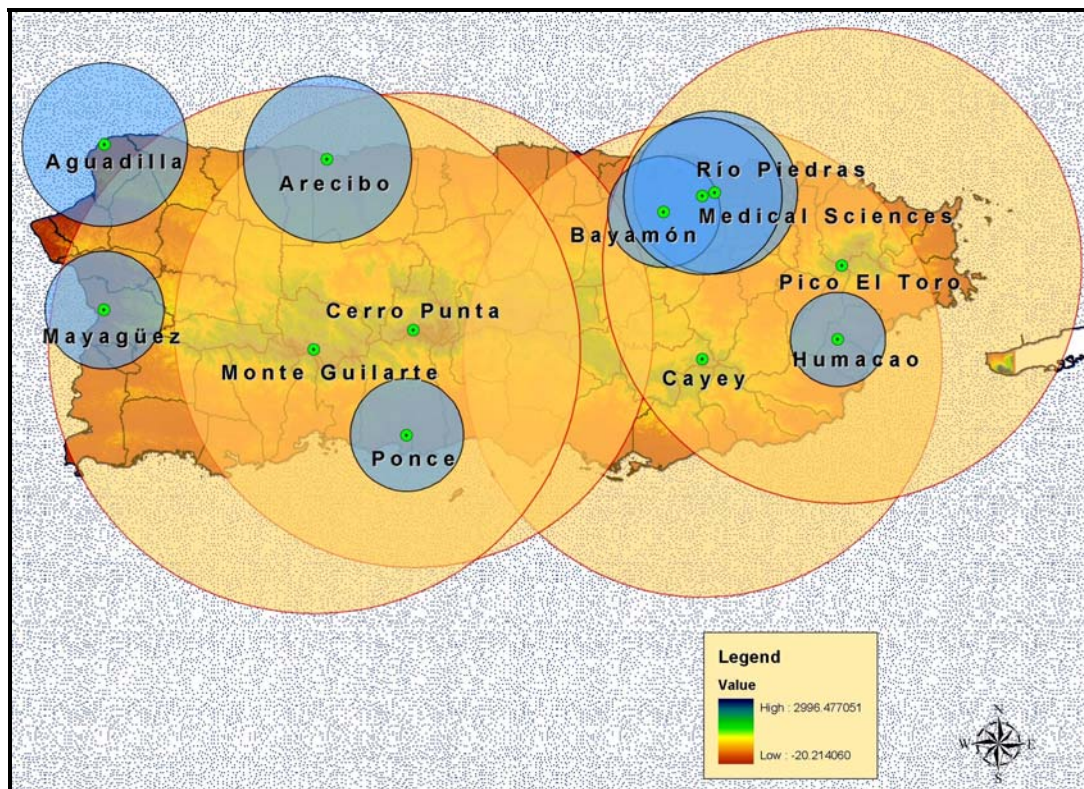


Figure 3.26. Radar network coverage using 1 Km maximum height circles and radars at the mountains.

The nodes on “Cerro Punta”, “Pico El Toro” and Cayey will need a range of 45 Km at an antenna tilt angle of 0.5 degrees, and the node in “Monte Guilarte” will have a range of 50 Km to get a complete coverage of the west area of the island.

Moreover, the antennas will be put on towers to surpass the other antennas from telecommunications companies. The height that the beam will reach from the ground with that range of coverage and the high height over sea level of the mountains will be 1.7 Km, 1.9 Km, 1.6 Km, and 1.3 Km for “Monte Guilarte”, “Cerro Punta”, “Pico El Toro”, and Cayey, respectively. Since the heights are over 1 Km, which is our area of interest and since the radars on top of the mountains will have to cover a high horizontal range, the curved earth problem will not be resolved and many information of the lower atmosphere will be lost. Furthermore, the radars will have high power transmitters to receive strong signals at that range. Hence, that option is not a good choice.

Another option is to reduce the antenna elevation angle in each campus to get a better coverage of the Island using towers to surpass the near obstacles. But a high tower will be required on top of the buildings. Table 3.1 shows the height of the tower to have an antenna inclination angle of 1° , surpassing the near obstacles. From the table, the campus that requires the tallest antenna tower (45 m) is Ponce due to the tall Ponce Judicial building located 400 m away from the campus library. Therefore, the radar antennas have to be mounted on the towers specified in Table 3.1 using the antenna inclination angle also specified. The installation of radars on top of the mountains will be necessary using the same locations used in the case of the high antenna tilt angles. The coverage map is shown in Figure 3.27 and shows that using that configuration the Island will have a complete coverage.

Table 3.1
Antenna tower and maximum range for a 1° antenna inclination angle

Campus	Tower Height on Top of the Building (m)	Maximum Range (Km)
Aguadilla	3.63	43.76
Arecibo	5.18	44.41
Bayamón	4.9	44.55
Humacao	7.9	45.07
Mayagüez	6.3	45.15
Medical Sciences	7.62	43.31
Ponce	45	46
Río Piedras	4.57	43.6

The problem with that arrangement is that the mountains will block the signal and will generate strong reflection signals as backscattering clutter for the receiver requiring more sensitive receivers in the radars.

Due to the fact that the clutter from the mountains is in a fixed position, its backscattering signal can be eliminated in the receiver. A method for eliminating the clutter from the mountains would be to eliminate the signal corresponding to the position where the mountains or the clutter is found, since each range position corresponds to a delay in the backscattering signal at the receiver. Taking into consideration that the mountains are stationary clutter and that atmospheric phenomena is in constant movement, another method to eliminate the clutter from the mountains in the received signal is to use Doppler measurements. The mountains are in a fixed position therefore, the backscattering signal will not have a Doppler frequency shift, while atmospheric phenomena will indeed cause a Doppler frequency shift in the signal. The implementation of the algorithm for clutter elimination is beyond the scope of this thesis. However, if the clutter from the mountains is not a major problem, this network configuration will be better than the other.

Hence, choosing the last option as the desired configuration, the radar backbone will have 6 nodes located in the University of Puerto Rico campuses of Aguadilla, Arecibo, Bayamón, Humacao, Mayagüez, and Ponce and 4 nodes located over the mountains “Monte Guilarte”, “Cerro Punta”, “Pico El Toro”, and one on top of a mountain in Cayey.

Each backbone node will require one radar or sensor in it. Since the interest is to obtain information from the atmospheric phenomena occurring at the lower atmosphere using polarimetric Doppler radars, the design at a block diagram level for the corresponding radar is explained in the next chapter.

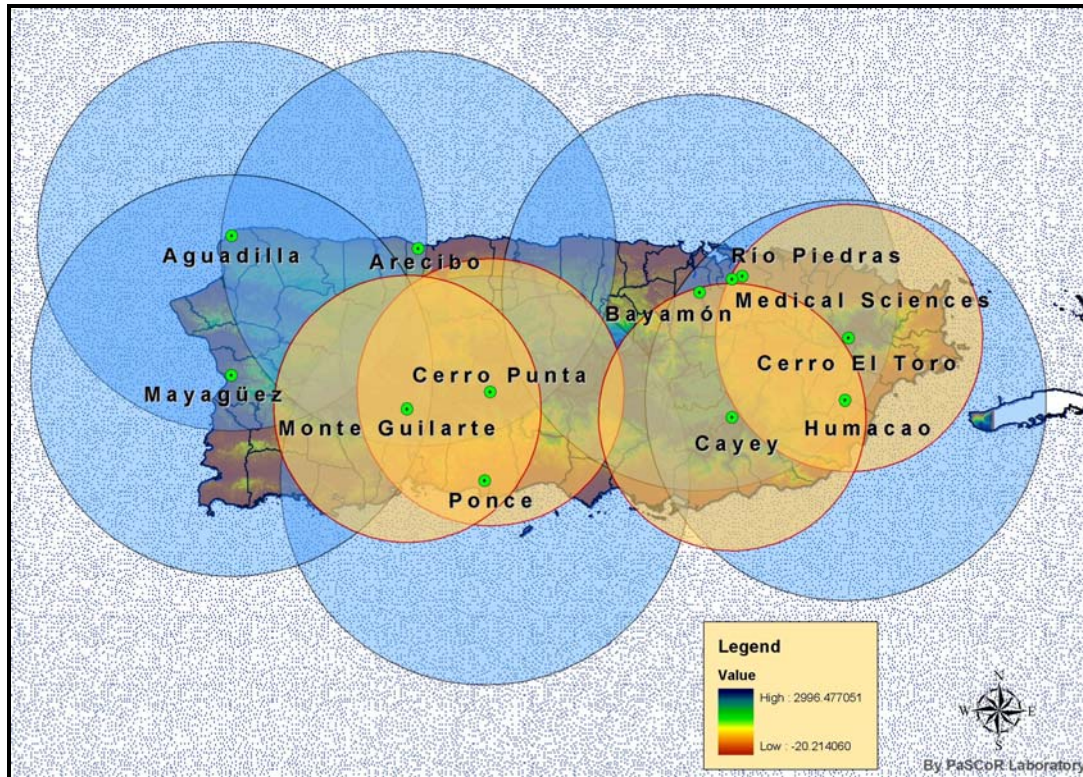


Figure 3.27. Radar network coverage using 1° antenna elevation angles at the campuses and radars at the mountains.

CHAPTER 4

NETWORK RADAR DESIGN

4.1 Overview

For each of the ten radar network nodes, a deployable polarimetric Doppler radar system is required. The first radar type will be constructed based on an inexpensive 25 KW magnetron X-Band single polarization Raytheon marine radar. The magnetron works at a frequency of 9.41 GHz, and it can be modified for weather events purposes. High frequencies will cause low power signals at the receiver. In addition, at this frequency the components will be relatively small, and good spatial resolution can be achieved. X-band is a high enough frequency to achieve a 1° beamwidth with a 2.1 m diameter antenna [11], which will be small enough to install in low profile towers.

The marine radar will be modified to have polarimetric and Doppler measurement capabilities. The polarimetric capability will be achieved by transmitting and receiving simultaneous vertical and horizontal electric field waves. The Doppler measurement capability will be achieved sampling the transmitted signal phase and comparing with the received signal phase. With these measurement capabilities, the radars will be capable to discriminate between rates, types, and amounts of precipitation. Moreover, the radars will be capable of correcting in time domain the system frequency drift caused by temperature variation in the magnetron using a bank of Gaussian filters, which will be discussed in Section 4.3.

The radar will be composed of interconnected subsystems including the transceiver, positioner and antenna, and data acquisition system. The modified radar transceiver was designed at a block diagram level for this thesis and discussed in the next section. In addition, the configuration for internal calibration is explained in Section 4.4.

4.2 Transceiver

The new X-Band radar transceiver design will be designed using some parts of the Raytheon marine radar transceiver, which is shown in Figure 4.1, and complete with new parts. From the Raytheon marine radar receiver, the parts that will be used in the new design are the magnetron, the isolator, the circulator and the TR limiter. The front end will not be used, since better sensitivity and dynamic range is required for the new applications. Given that the new transceiver will have polarimetric capabilities, one horizontal and one vertical channel are required.

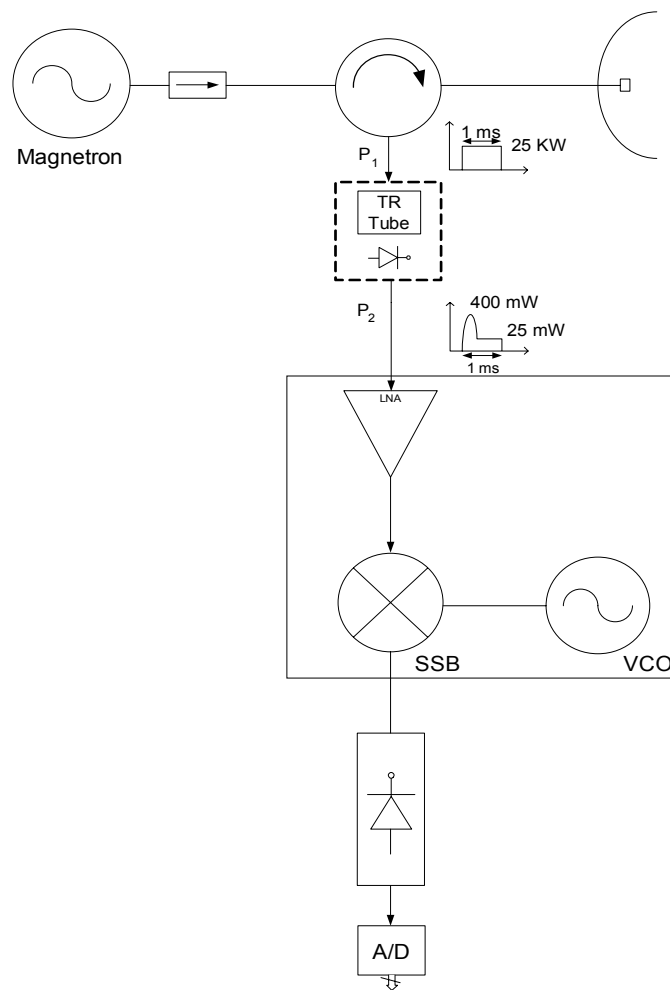


Figure 4.1. Raytheon marine radar transceiver

4.2.1 System description

The magnetron transmits a peak power of 25 KW at a center frequency of 9.41 GHz. The isolator protects the magnetron from any returning signal, sending the received signal to a load connected in the other port. The limiter is used to protect the receiver from strong received signals and is comprised of a gas discharge limiter, which attenuates the leakage of the transmitted signal, and a pin diode. The output of the limiter is limited to a maximum peak power of 400 mW in the first half of the pulse and a constant power of 25 mW in the second half as Figure 4.1 shows.

Using those parts and the new parts, the new transceiver will look as in Figure 4.2. The pulse is generated modulating the magnetron's continuous output with a high voltage modulator. The magnetron is protected with the isolator obtained from the Raytheon marine radar. The pulse enters to a component called the magic tee, which is a power divider with a horizontally and a vertically polarized output. Then the horizontally and vertically polarized pulses are combined in the orthomode transducer (OMT) resulting in a 45° elliptically polarized pulse, which will be sent through the dual-polarization antenna. A sample of the signal is taken in the transmission process for calibration purposes. Waveguides are used in all transmission steps since high power signals are being managed.

For reception, the backscattered signal is received at the antenna. Then the signal is divided into a horizontally and a vertically polarized signal by the OMT and sent into the receiver through the circulator. In the receiver, the first part encountered is the TR limiter, which protects the receiver front end from strong signals. Next, a switch for isolation purposes and a 20 dB coupler are used for internal calibration, which will be discussed in Section 4.4. The next part after the coupler is a box containing a low noise amplifier, which establishes the noise figure of the receiver. Then, a mixer used to lower the frequency from 9.41 GHz to 60 MHz using a 9.35 GHz oscillator, and a bandpass filter to filter out the signal images occurring in the mixing process will be included in the same box. That configuration is called a superheterodyne receiver.

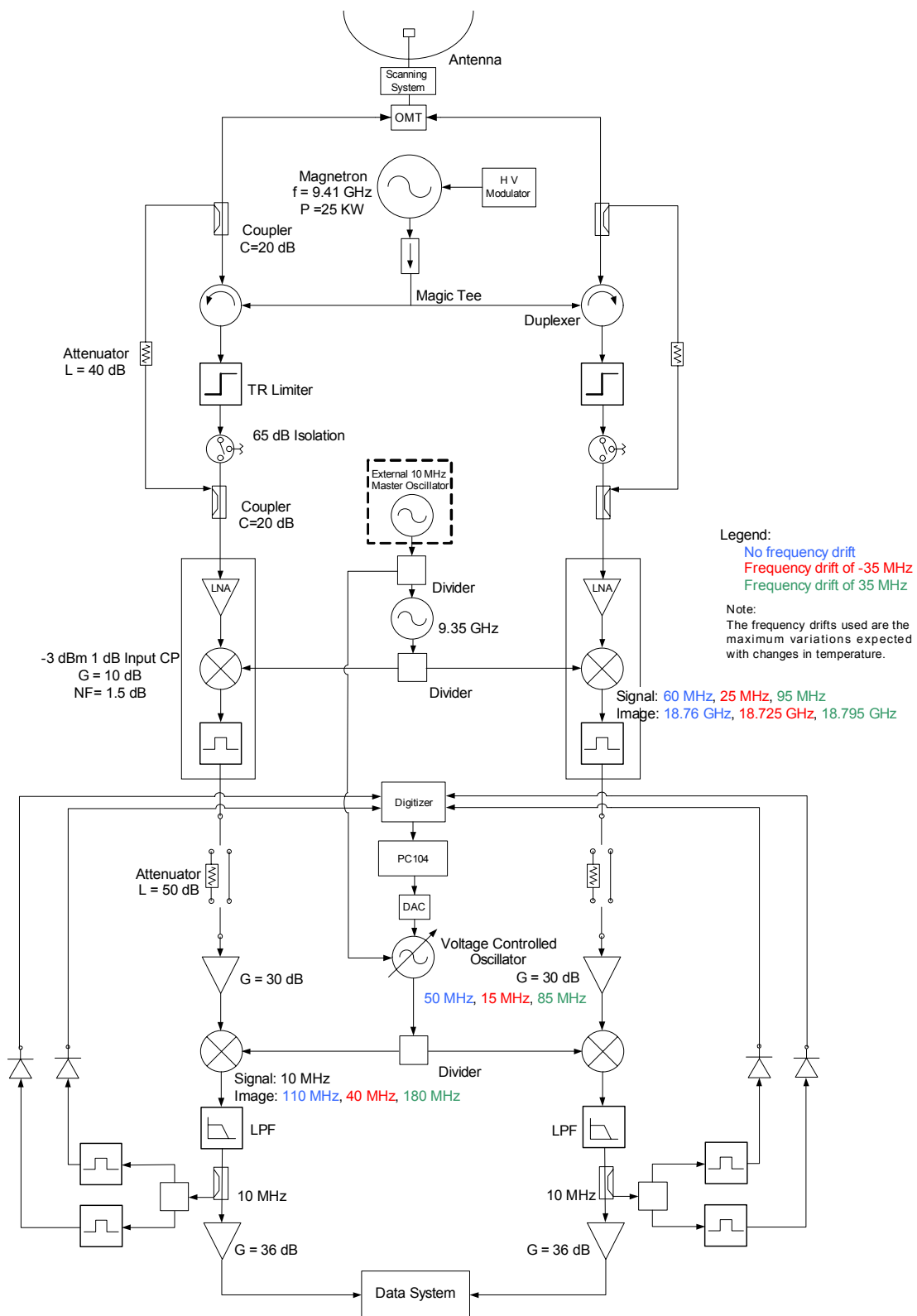


Figure 4.2. Network radar transceiver block diagram

After the superheterodyne box, a switch with a 50 dB load is used to attenuate the leakage signal introduced in the receiver at transmission mode to protect the data system. Since the data system has a frequency of operation of 10 MHz, the signal is mixed again to get the desired 10 MHz at the data system input and filtered with a lowpass filter to reject the images. The signal is amplified in two stages of 30 dB and 36 dB of gain to increase the noise power of the system to 10 dB above the minimum input power level of the data system (DSP Board GVA-290), which is -55 dB.

Before the second amplification, a 20 dB coupler is used to sample the 10 MHz signal, which is divided by a 2-way power divider. The two signals are passed through two Gaussian bandpass filters and two log-detectors and processed in the computer (PC104). Using Gaussian shape filters, the magnetron thermal frequency drift can be estimated and corrected, supplying the second mixing stage (10 MHz) with a voltage controlled oscillator (VCO) or a direct digital synthesis (DDS) source. Both will vary the output frequency. In the VCO case, the output frequency will vary with the input power and in the DDS case the output will be reprogrammable by the computer. Finally, the oscillators used in the mixers are synchronized by a 10 MHz crystal master oscillator.

The antenna will be mounted in a positioner, which will be controlled to point out precise targets in azimuth and elevation angles at a complete 360° swath. A summarized list and price table of the radar components is in Appendix C.

4.2.2 System specifications

The required network radar will be a pulsed radar system. The magnetron will be pulsed in 1 μ s duration pulses using both vertical and horizontal electric fields at a frequency of 9.41 GHz. A maximum unambiguous range of 46 Km is required for the node with the larger coverage area (Ponce campus). This is the maximum range or distance from the radar the beam can reach before another pulse can be transmitted. This range establishes the required pulse repetition frequency (PRF), which is the

frequency between pulses, and also establishes the maximum unambiguous velocity, which is the maximum velocity that can be measured with minimum error. The unambiguous range and unambiguous velocity are given by

$$R_{\max} = \frac{c}{2PRF} \quad (4.1)$$

$$v_{\max} = \pm \frac{\lambda PRF}{4} \quad (4.2)$$

where c is the free-space speed of light and λ is the transmitted signal wavelength. From Equation 4.1 and with a maximum unambiguous range of 46 Km, a PRF of 3.26 KHz is required. Using the PRF in Equation 4.2, the maximum unambiguous velocity will be ± 23.91 m/s, which is a low unambiguous velocity. Since, in tropical storms, hurricanes and other atmospheric phenomena high velocity precipitation occurs, higher unambiguous velocities are required. The method of staggered pulse pair [11] can be used to increase the maximum unambiguous velocity of the radar. That method requires the use of a higher PRF pulse pair in the transmission in combination with the original PRF. This gives more weight to the higher PRF in the computation of the maximum unambiguous velocity as Equation 4.3 shows.

$$v_{\max} = \pm \frac{\lambda}{4(PR_2^{-1} - PR_1^{-1})} \quad (4.3)$$

As mentioned earlier, the magnetron has a thermal frequency drift from the center frequency. For that reason, the system bandwidth cannot be matched using a matched filter of 1 MHz of bandwidth (1 μ s pulse bandwidth). A system bandwidth of 5 MHz was calculated to account for thermal frequency drift variations, making the receiver

vulnerable to frequency changes up to ± 2.5 MHz. The problem of using a wider bandwidth is that more noise will enter into the receiver.

To obtain the system dynamic range, the system noise floor has to be computed using the noise figure of the cascade components encountered before the radar front-end (low noise amplifier box) in Equation 4.4. Figure 4.3 shows the cascade components with their respective gain and noise figure.

$$F_{sys} = F_1 + \frac{F_2 - 1}{G_1} + \frac{F_3 - 1}{G_1 G_2} \quad (4.4)$$

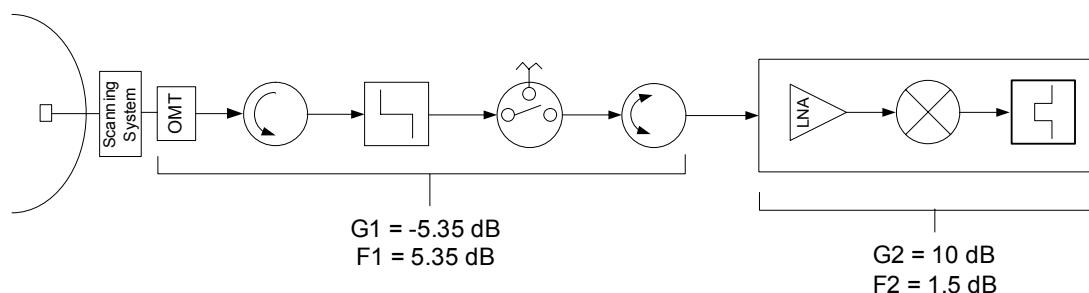


Figure 4.3. Radar noise figure calculation elements

Using Figure 4.3 and Equation 4.4 the system noise figure (F_{sys}) results in 6.85 dB. With the system noise figure already calculated, the noise power floor at the input of the low noise amplifier box can be calculated as

$$P_N = k(F_{sys} - 1)T_0 B \quad (4.5)$$

where B is the system bandwidth T_0 is the ambient temperature (290 K) and k is the Boltzmann constant (1.38066×10^{-23}). Hence, using the system noise temperature calculated earlier in Equation 4.5 an input noise power of -101.14 dBm results. Using a front-end box with a 1 dB compression point input of -3 dB design by a company

(MITEQ), the system dynamic range will be of -98.14 dB, which is a good dynamic range that makes the receiver very sensitive.

4.3 Magnetron thermal frequency drift control method

A magnetron is a self-contained microwave oscillator, where electric and magnetic fields are used to produce the high power output required in radar systems. It is composed of cavities that control the output frequency. Since the cavities expand as the temperature increases, the output frequency of the magnetron changes gradually, causing errors in the measurements, especially in Doppler frequency measurements.

In the case of Raytheon marine radar's magnetron (M1458), frequency changes with temperature were measured at UMass. The data is shown in Figure 4.4. The plot shows that the frequency varies at a rate of 0.2284 Hz per °C, which results in a frequency drift of 4.5 MHz in an interval of 19.7°. Since, the rate of variation is not high and the thermal process is very slow, the frequency drift can be controlled using a feedback method.

A Gaussian filter bank will be used to control the magnetron thermal frequency drift. The method consists in taking a sample of the signal entering the DSP board, divide it in equal parts with a 2-way power divider, pass the two signals through two equal bandpass Gaussian filters and detect the signals' envelope using two log-detectors as shown in Figure 4.5. Next, the signal will be digitized, using a 10-bit digitizer and processed in the computer (PC104) to determine the drift of the signal. The computer output will be sent to a voltage-controlled oscillator after signal conversion to analog with a digital to analog converter. Then, the VCO with the input voltage will be capable of changing the mixing frequency and correct the thermal frequency drift.

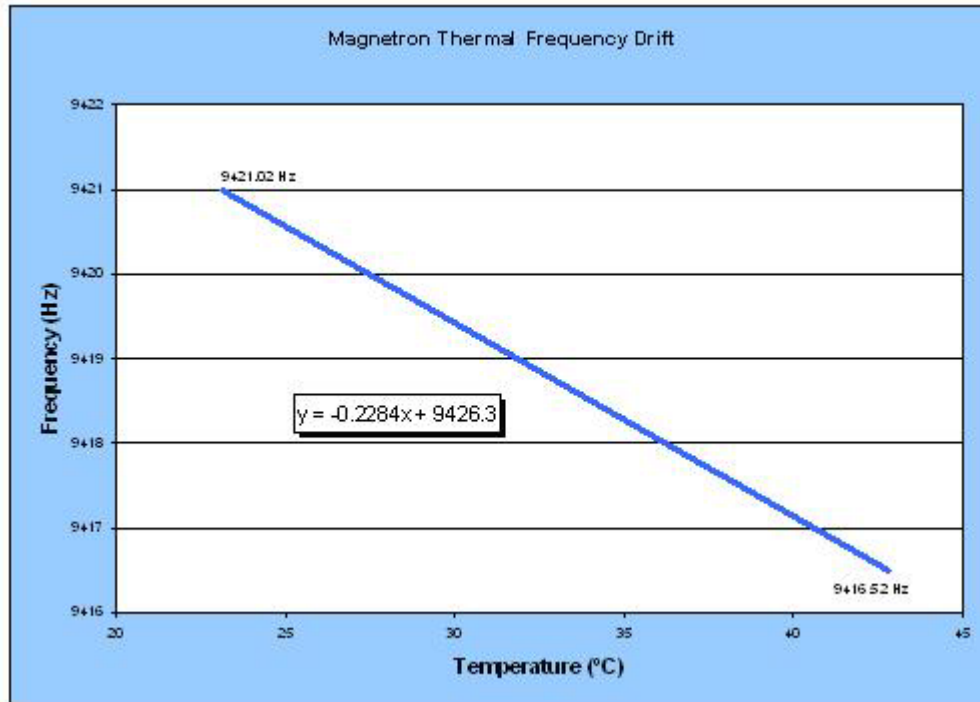


Figure 4.4. Plot of the magnetron's thermal frequency-drift

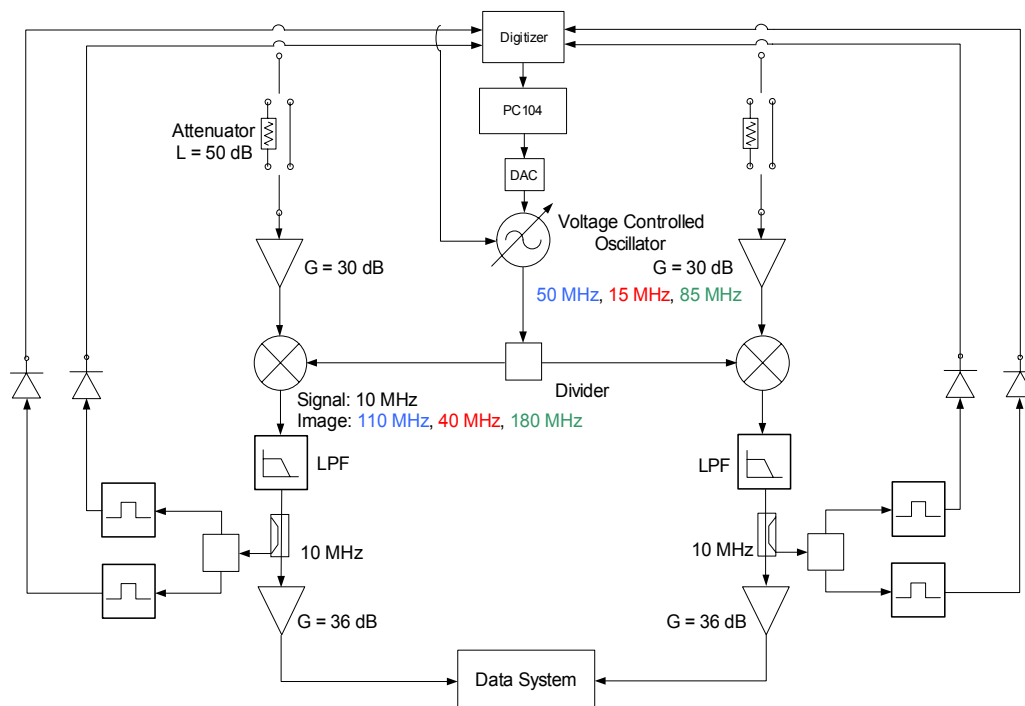


Figure 4.5. Block diagram for the magnetron thermal-frequency-drift control method

The two Gaussian filters were simulated and are shown in Figure 4.6. Since the filter bandwidth is defined up to the points where the filter magnitude is 3 dB below the maximum voltage, for the method to work, one of the Gaussian filters will have the right -3 dB point of at the center frequency (10 MHz in our case) and the other its left -3 dB point, as shown in Figure 4.6. In the figure, the filters have a bandwidth of 7 MHz to account for frequency drifts up to ± 7.5 MHz. This bandwidth is wide enough to correct the frequency drift.

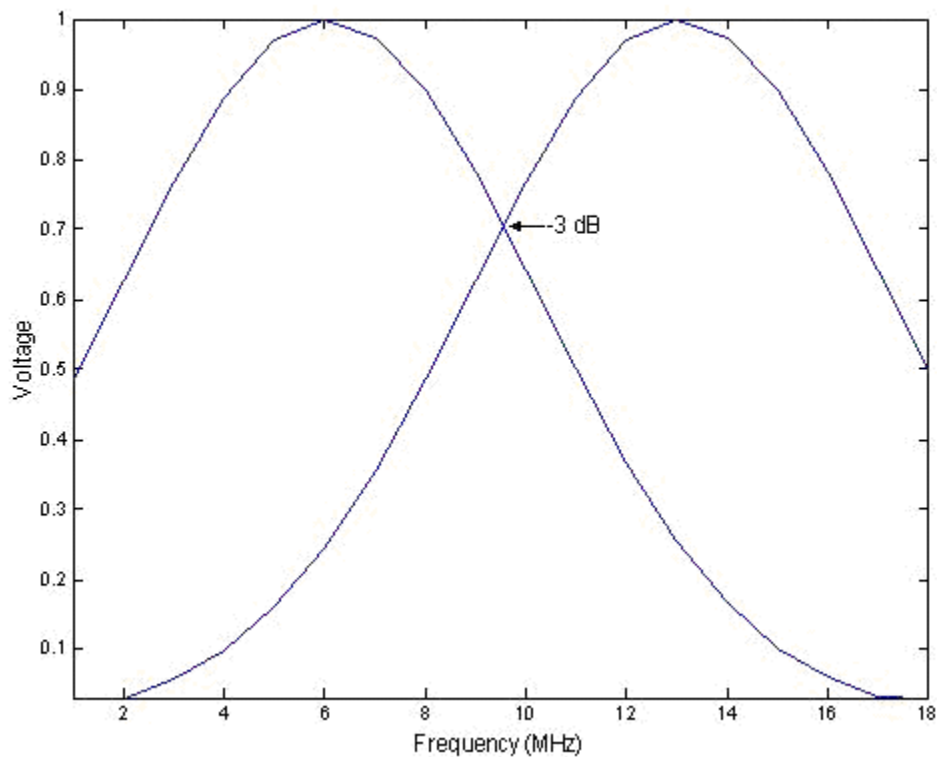


Figure 4.6. Gaussian filters representation plot

Computing the logarithm from both filters, differentiating and plotting them results in Figure 4.7. The figure shows that the plot has a linear behavior with a certain bandwidth. The bandwidth of the linear part of the curve depends on the bandwidth of the filters. As the bandwidth of the filters increases, the bandwidth of

the linear part also increases. Since the logarithmic difference of the filters follows a linear pattern, a relationship between thermal frequency drift and the filters' output voltage can be obtained to correct the problem.

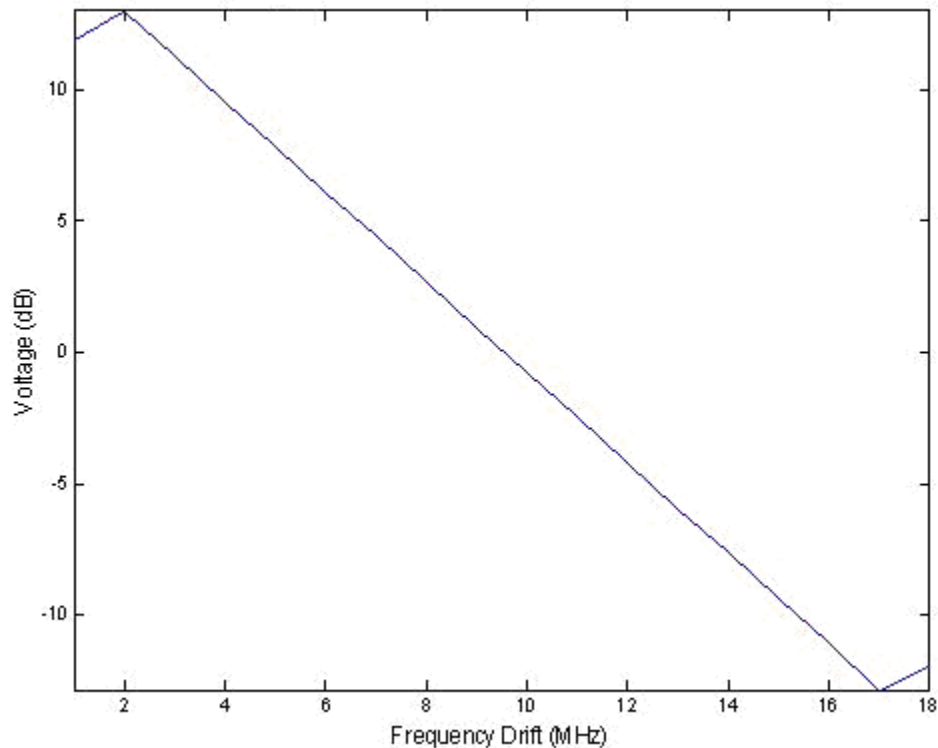


Figure 4.7. Logarithmic subtraction of the Gaussian filters

4.4 Internal calibration

The internal and external calibrations of the radar system are important parts or processes in obtaining accurate measurements. Both are required for a high reliability paradigm. For external calibration, targets with known radar cross-section like corner reflectors and metal spheres are used to obtain the radar constant, which will be used to process the backscattering information. On the other hand, the

internal calibration provides continuous monitoring of most of the radar parameters, such as transmit power and receiver gain [12].

When the leakage signal is out of phase with the calibration loop signal, the worst-case error is produced and can be expressed as [12],

$$e_{cal}(dB) = \left| 20 \log_{10} \left(1 - \sqrt{\frac{P_{leak}}{P_{cal}}} \right) \right| \quad (4.6)$$

where P_{leak} is the power leaking to the receiver and P_{cal} is the power from the calibration loop signal. Equation 4.6 is plotted in Figure 4.8 as a function of the logarithm of the P_{cal}/P_{leak} ratio. The goal of the calibration loop is to achieve an error less than 0.1 dB, which corresponds to a leakage power of 40 dB below the calibration signal, but an error of 0.25 dB, which requires a leakage power signal 30 dB below the calibration signal, is acceptable [12].

A calibration loop block diagram was designed for the radar to achieve the maximum calibration error of 0.25 dB and is shown in Figure 4.9. First, a 20 dB coupler is used to sample the transmitted power and to obtain the calibration power signal. In the same calibration loop, an X-Band detector diode is used to monitor the transmit power magnitude and phase for Doppler measurements. Since the detector is a broadband component, the frequency drift from the center frequency of the magnetron cannot be measured. Next, a load is placed in the calibration path to decrease the power that enters the receiver front-end to 3 dB below the 1 dB compression point, and work within the linear region. Finally, another 20 dB coupler is used to inject the calibration signal into the receiver in transmission mode.

On the other hand, since circulators are not perfect isolators, some leakage of the transmitted power slips through the receiver. Given that we want to reduce the power of the leakage signal to obtain the desired 30 dB ratio, an absorptive isolator switch is used. In addition, a constant and stable external power source is injected using a noise diode to constantly monitor the receiver gain.

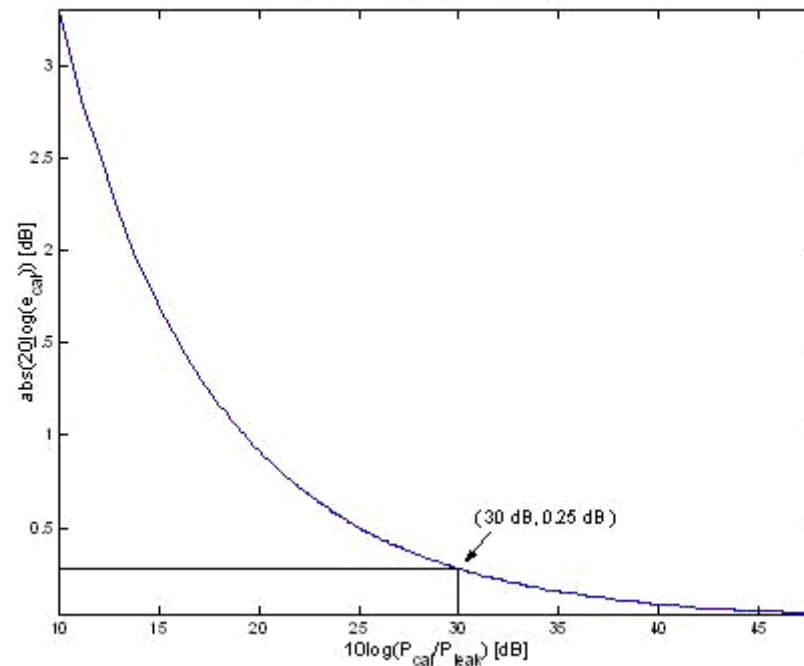


Figure 4.8. Internal calibration error plot

In our case, the 1 dB compression point of the front end is -3 dBm, the transmitted power is 74 dBm, and the maximum power that comes out through the TR limiter (P_2) is 26 dBm. Using those specifications, a 40 dB attenuator (L) and a 62 dB isolator switch are required to achieve the 30 dB P_{cal}/P_{leak} ratio. The specifications are summarized in Table 4.1 for five different front-end 1 dB compression points.

Table 4.1
Calibration loop specifications

Front End 1 dB CP	Pcal	Pulse Peak Power	L	Pleak	Switch Isolation
-25 dBm	-28 dBm	74 dBm	62 dB	-58 dBm	84 dB
-10 dBm	-13 dBm	74 dBm	47 dB	-43 dBm	69 dB
-5 dBm	-8 dBm	74 dBm	42 dB	-38 dBm	64 dB
-3 dBm	-6 dBm	74 dBm	40 dB	-36 dBm	62 dB
0 dBm	-3 dBm	74 dBm	37 dB	-33 dBm	59 dB

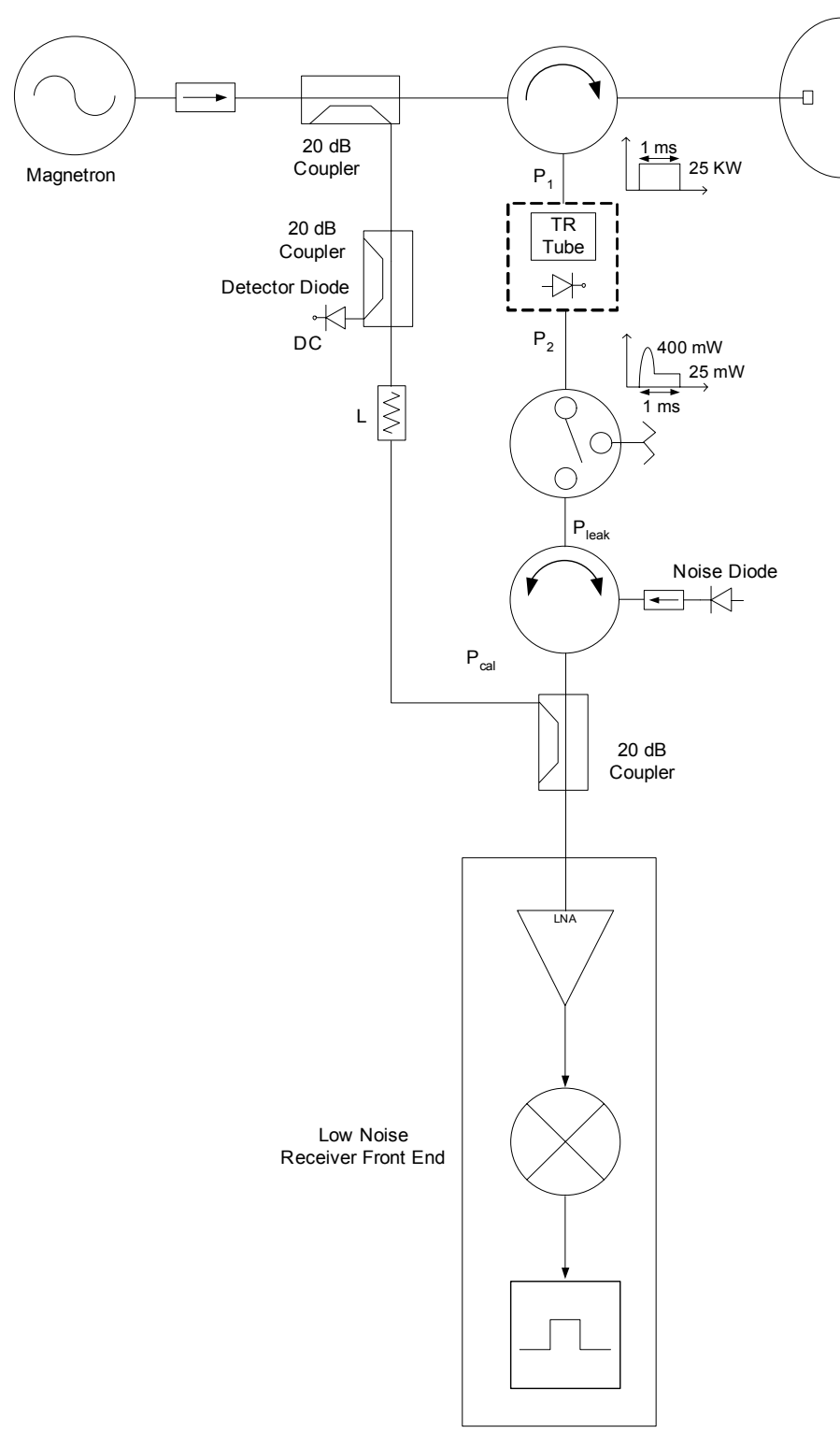


Figure 4.9. Radar calibration loop block diagram

CHAPTER 5

CONCLUSIONS AND FUTURE WORK

5.1 Summary

This thesis has described the Puerto Rico deployable radar network site survey and a preliminary radar design, which will be part of the first collaborative and adaptive radar network system to measure lower atmospheric phenomena in Puerto Rico.

The effect of the Earth's curvature on beam propagation was described. A method to survey the eleven campuses of the University of Puerto Rico backbone and the Tilson farm at UMass was explained. Each surveyed site fixed offset antenna elevation angle and location is justified with *in situ* measured data and satellite digital data. The expected network radar backbone range of coverage was computed and plotted using two derived equations describing the curved Earth effect on beam propagation, and sounding data. For the network only six of the eleven campuses of the University of Puerto Rico (Aguadilla, Arecibo, Bayamón, Humacao, Mayagüez, and Ponce) were chosen as nodes. In addition, four nodes over the mountains were digitally accessed to get a complete coverage of the Island because the campuses are located at low heights compared to the high mountains in the center of the Island, requiring high antenna tilt angles and reducing the radar coverage area.

The desired polarimetric Doppler network radar RF transceiver was designed and explained at a block diagram level, modifying a single channel Raytheon marine radar. The method of the Gaussian filter bank for magnetron thermal frequency drift correction was discussed. Finally the radar internal calibration loop, which will be used for stability and system performance evaluation was designed and explained at block diagram level.

The network will serve as a complement for the current NEXRAD system.

5.2 Future work

The first step is to acquire the permits from the Federal Communications Commission (FCC) to use the X-Band part of the spectrum and to install the radars in the selected nodes.

With the polarimetric Doppler radar already designed at a block diagram level, the next step is its construction as well as the construction of the data system as part of my PhD work at the University of Massachusetts at Amherst. When the radar is constructed, it will be used in the established nodes to begin the data collection for the Puerto Rico test-bed.

In addition, the design of other radar systems using klystron tubes to transmit the power will be taken into consideration.

REFERENCES

- [1] M. I. Skolnik, *Introduction to Radar Systems*, 3rd ed. New York, NY. McGraw-Hill, 1980.
- [2] V. N. Bringi and V. Chandrasekar, *Polarimetric Doppler Weather Radar Principles and Applications*, Cambridge, UK. Cambridge University Press, 2001. 636 pp.
- [3] T. Schuur, *National Severe Storms Laboratory, Polarimetric Radar Research*. <http://www.nssl.noaa.gov/~schuur/radar.html>. February 2003.
- [4] A. V. Ryzhkov and D. S. Zrnich, "Heavy Precipitation Measurements at S-band with a Polarimetric Radar", *IEEE Transactions Geoscience and Remote Sensing*, Vol. 1 , Aug 1994. pp. 19 -21
- [5] J. B. Mead, A. L. Pazmany, S. M. Sekelsky and R. E. McIntosh, "Millimeter-Wave Radars for Remotely Sensing Clouds and Precipitation", *Proceedings of the IEEE*, Vol. 82, No. 12, December 1994.
- [6] H. W. J. Russchenberg and L. P. Ligthart, "Polarimetric Studies of Hydrometeors with the Delft Atmospheric Research Radar", *International Conference on Antennas and Propagation*, Vol. 2, No. 301, pp. 83 -87, Apr 1989.
- [7] D. S. Zrnich, *Simultaneous Differential Polymetric Measurements and Co-Polar Correlation Coefficient Measurement*, United States Patent, 5,500,646, March 1996.
- [8] Zahrai and D. S. Zrnich, "Implementation of Polarimetric Capability for the WSR-88D (NEXRAD) Radar", *Proceedings of the IEEE Aerospace and Electronics Conference*, Vol. 1, Jul 1997. pp. 346-352
- [9] J. M. Trabal-del Valle, J. G. Colom-Ustáriz, S.L. Cruz-Pol, and S. M. Sekelsky, "Puerto Rico Deployable Radar Network Design; Site Survey", *IGARSS 03*, France, 2003.
- [10] F. T. Ulaby, R. K. Moore and A. K. Fung, *Microwave Remote Sensing Active and Passive*, Vol. 1, Addison-Wesley Publishing Company, Reading, Massachusetts, 1981. 456 pp.

- [11] F. Junyent, "The Design and Initial Field Deployment of an X-Band Polarimetric Doppler Weather Radar", M.S. Thesis, University of Massachusetts at Amherst, September 2003. 102 pp.
- [12] M. Bergada, "Design and Implementation of a Low Noise Front-End and Internal Calibration Loop for a KA- Band Cloud Radar", M.S. Thesis, University of Massachusetts at Amherst, May 2001. 95 pp.

BIBLIOGRAPHY

F. Solheim, J. R. Godwin, E. R. Westwater, Y. Han, S. J. Keihm, K. Marsh, and R. Ware, "Radiometric Profiling of Temperature, Water Vapor and Cloud Liquid Water Using Various Inversion Methods", *Radio Science*, Vol. 33, March-April 1998. pp. 393-404

G. A. Sadowy, A. C. Berkun, W. Chun, E. Im and S. L. Durden, "Development of an Advanced Airborne Precipitation Radar", *Microwave Journal*, January 2003. pp. 84-98

G. W. Stimson, *Introduction to Airborne Radar*, 2nd ed. Raleigh, NC. SciTech Publishing, 1998. 576 pp.

H. Sauvageot, *Radar Meteorology*, Norwood, MA. Artech House, 1992. 366 pp.

M. A. Fischman, A. C. Berkun, F. T. Cheng and W.W. Chun, "Design and Demonstration of an Advanced On-Board Processor for the Second -Generation Precipitation Radar", *Proceedings of the IEEE Aerospace Conference*, Vol. 2, March 8-15 1997. pp. 1067-1075

M. I. Skolnik, *Radar Handbook*, 2nd ed. New York, NY. McGraw-Hill, 1990. Chapter 23. 11 pp.

R. J. Doviak, D. S. Zrnić, *Doppler Radar and Weather Observations*, 2nd ed. London, UK. Academic Press, 1993. 562 pp.

S. M. Sekelsky and R. E. McIntosh, "Cloud Observatons with a Polarimetric 33 GHz and 95 GHz Radar", *Meteorology and Atmospheric Physics*, Springer-Verlag, 1996. pp. 123-140

APPENDIX A
SURVEYED CAMPUSES LOCATION

Aguadilla campus

Aguadilla campus is located at Belt Street Old Ramey Base at Aguadilla, Puerto Rico. The survey was made on top of the new library building. Figure 3.1 shows an image from satellite IKONOS of the campus. The survey point is marked on the image.



Figure A.1. University of Puerto Rico, Aguadilla Campus. Image from satellite IKONOS.

Arecibo campus

Arecibo campus is located at the Hato Abajo Suburb in the Hoyo Los Santos Sector in Road 653 Km 0.8 at Arecibo, Puerto Rico. The survey was made on top of the humanities department building. Figure 3.2 shows an image from satellite IKONOS of the campus. The survey point is marked on the image.



Figure A.2. University of Puerto Rico, Arecibo Campus. Image from satellite IKONOS.

Bayamón campus

Bayamón campus is located at 174 Minillas Industrial Park Road 170 at Bayamón, Puerto Rico. The survey was made on top of the new student center building. Figure 3.3 shows an image from satellite IKONOS of the campus. The survey point is marked on the image.

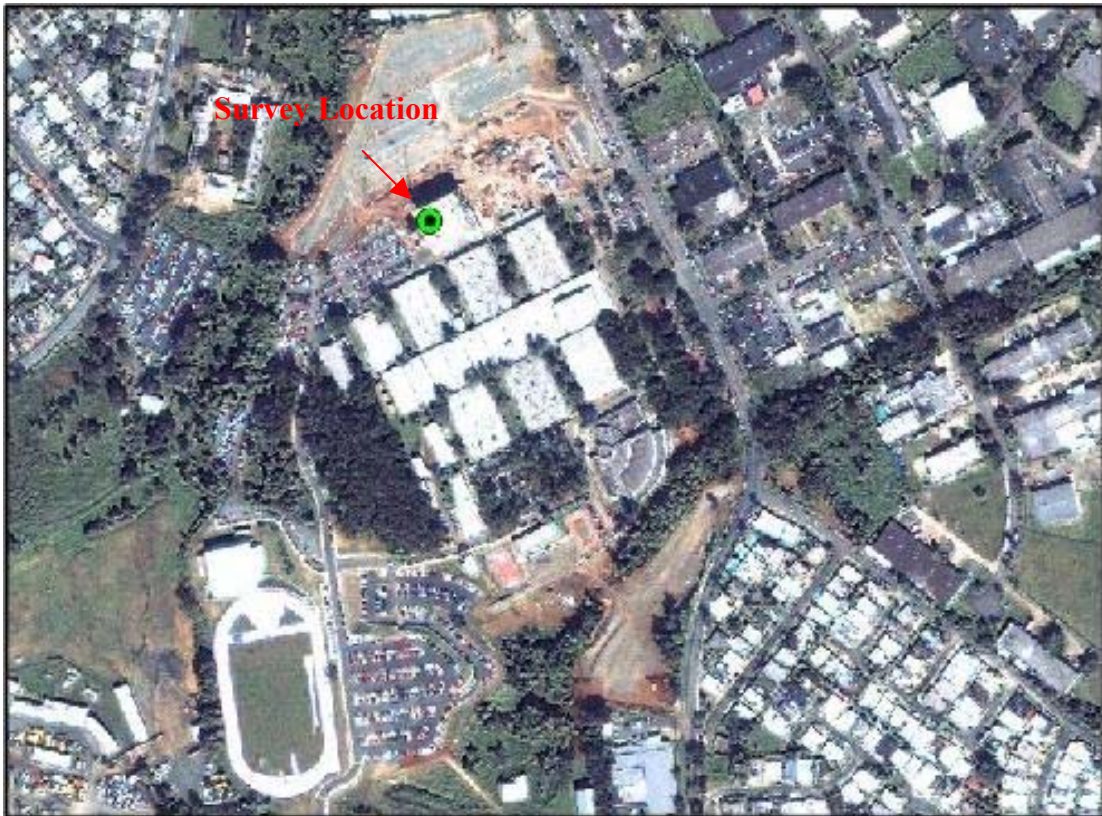


Figure A.3. University of Puerto Rico, Bayamón Campus. Image from satellite IKONOS.

Carolina campus

Carolina campus is located at 2100 South Avenue at Carolina, Puerto Rico. The survey was made on top of the natural sciences laboratories building. Figure 3.4 shows an image from satellite IKONOS of the campus. The survey point is marked on the image.



Figure A.4. University of Puerto Rico, Carolina Campus. Image from satellite IKONOS.

Cayey campus

Cayey campus is located at 205 Antonio R. Barceló Avenue at Cayey, Puerto Rico. The survey was made on top of the Miguel Melendez Muñoz sciences building. Figure 3.5 shows an image from satellite IKONOS of the campus. The survey point is marked on the image.

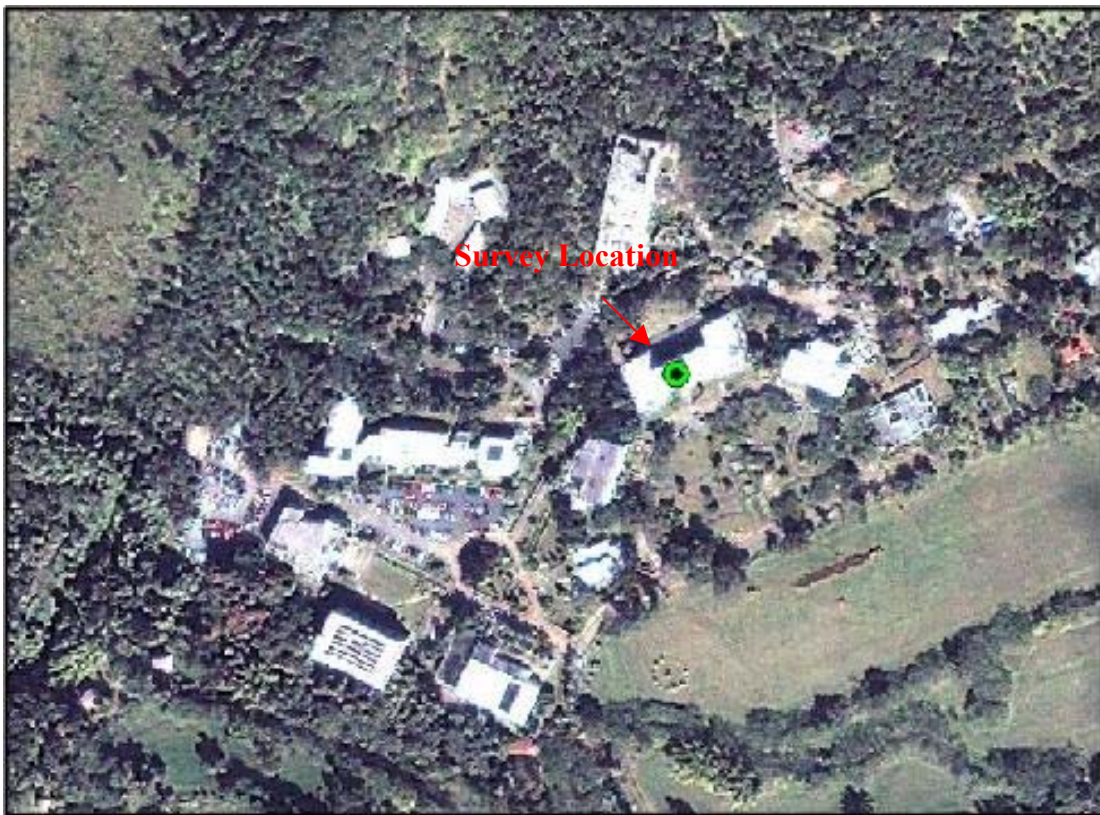


Figure A.5. University of Puerto Rico, Cayey Campus. Image from satellite IKONOS.

Humacao campus

Humacao campus is located at 100 Road 908 at Humacao, Puerto Rico. The survey was made on top of the library building. Figure 3.6 shows an image from satellite IKONOS of the campus. The survey point is marked on the image.



Figure A.6. University of Puerto Rico, Humacao Campus. Image from satellite IKONOS.

Mayagüez campus

Mayagüez campus is located at Post Street at Mayagüez, Puerto Rico. The survey was made on top of the Chemistry building. Figure 3.7 shows an image from satellite Landsat of the campus. The survey point is marked on the image.



Figure A.7. University of Puerto Rico, Mayagüez Campus. Image from satellite Landsat.

Medical Sciences campus

Medical Sciences campus is located at Medical Center Area at San Juan, Puerto Rico. The survey was made on top of the Central Offices building. Figure 3.9 shows an image from satellite IKONOS of the campus. The survey point is marked on the image.

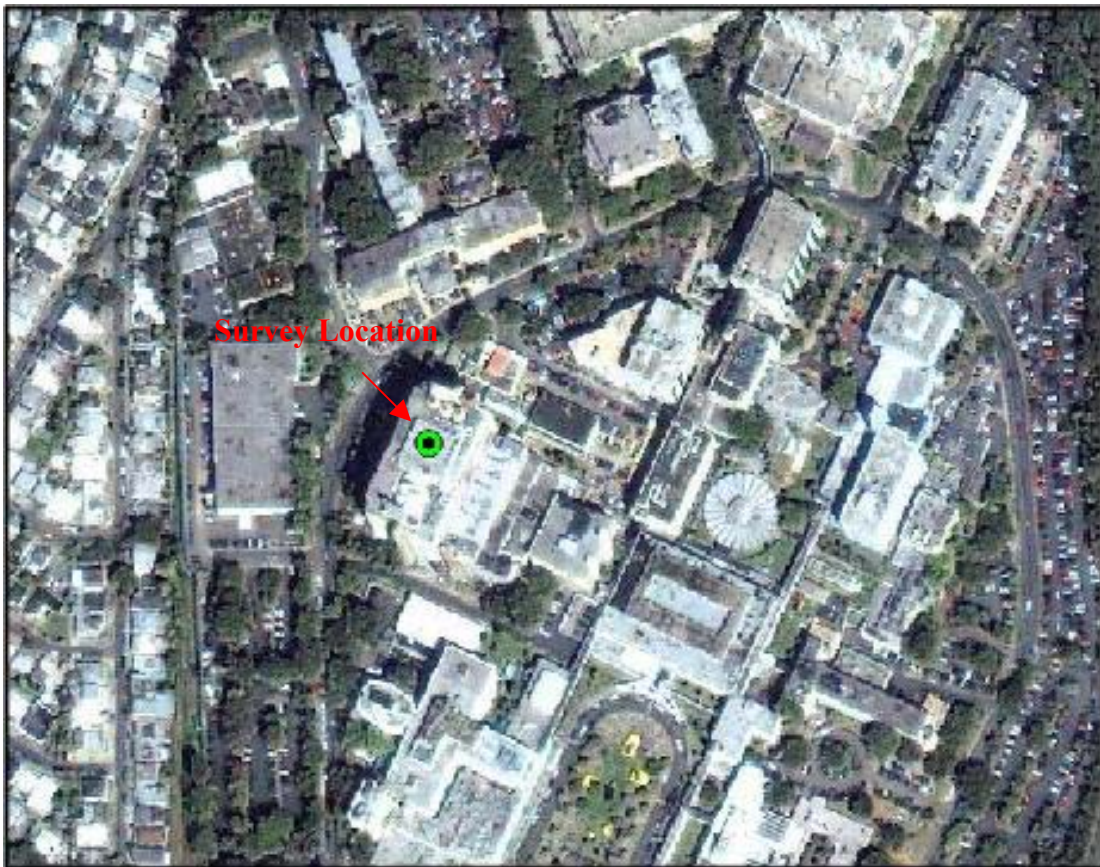


Figure A.9. University of Puerto Rico, Medical Sciences Campus. Image from satellite IKONOS.

Ponce campus

Ponce campus is located at 2151 Santiago de los Caballeros Avenue at Ponce, Puerto Rico. The survey was made on top of the library building. Figure 3.8 shows an image from satellite Landsat of the campus. The survey point is marked on the image.



Figure A.8. University of Puerto Rico, Ponce Campus. Image from satellite Landsat.

Río Piedras campus

Río Piedras campus is located at 38 Ponce de León Avenue at San Juan, Puerto Rico. The survey was made on top of North Tower building. Figure 3.10 shows an image from satellite IKONOS of the campus. The survey point is marked on the image.



Figure A.10. University of Puerto Rico, Río Piedras Campus. Image from satellite IKONOS.

Utado campus

Utado campus is located at Road 10 Km. 52.2 Salto Arriba Suburb at Utado, Puerto Rico. The survey was made on top of Building B. Figure 3.11 shows an image from satellite IKONOS of the campus. The survey point is marked on the image.



Figure A.11. University of Puerto Rico, Utado Campus. Image from satellite IKONOS.

APPENDIX B
CAMPUSES SURVEY DATA

Aguadilla Campus Survey Data - Library Building					
NAD27					
18 29 46.96 N					
67 08 14.93 W					
Azimuth Angle (°)	Minimum Elevation Angle (°)	Azimuth Angle (°)	Minimum Elevation Angle (°)	Azimuth Angle (°)	Minimum Elevation Angle (°)
0	1	120	2.2	240	1.8
5	1	125	1.5	245	2.1
10	1	130	3.3	250	2.3
15	1	135	1.5	255	1.8
20	1	140	1.8	260	1.2
25	1	145	2.4	265	2.4
30	1	150	1.8	270	1.6
35	1	155	1.6	275	1.8
40	1.1	160	2.5	280	2.4
45	1	165	2.4	285	1.2
50	1.2	170	2.5	290	4
55	1	175	2.4	295	1
60	1	180	2.6	300	1
65	1	185	2.5	305	1
70	1	190	2.4	310	1
75	1	195	2.4	315	1
80	1	200	2.2	320	1
85	1	205	2.7	325	1
90	1.2	210	2.4	330	1
95	1.7	215	2.4	335	1
100	1.4	220	2.2	340	1
105	1	225	2.2	345	1
110	3.4	230	1.9	350	1
115	2.1	235	2	355	1

Table B.1. Aguadilla Campus Survey Data

Arecibo Campus Survey Data - Humanities Department Building					
NAD27					
18 28 00.05 N					
66 44 29.06 W					
Azimuth Angle (°)	Minimum Elevation Angle (°)	Azimuth Angle (°)	Minimum Elevation Angle (°)	Azimuth Angle (°)	Minimum Elevation Angle (°)
0	1.7	120	4.2	240	1.5
5	1.8	125	2.6	245	1.8
10	2.3	130	3.2	250	1.5
15	2.4	135	2.8	255	2.1
20	2.9	140	2.8	260	1.5
25	3.3	145	3	265	1.1
30	6.6	150	2.8	270	1.2
35	5.9	155	3.2	275	1
40	4.6	160	3.3	280	1
45	4.1	165	3.1	285	1
50	4.2	170	3	290	1
55	3.4	175	2.7	295	2.2
60	4.7	180	2.9	300	1
65	4.6	185	2.6	305	1
70	3.9	190	2.9	310	1
75	4.4	195	2.4	315	1
80	4.1	200	3.1	320	1.3
85	5	205	2.7	325	1.6
90	3	210	2.4	330	2.2
95	3.5	215	2.2	335	1
100	2.8	220	2.2	340	1
105	2.7	225	2	345	1.6
110	3.5	230	1.8	350	2.2
115	4.1	235	1.8	355	3.1

Table B.2. Arecibo Campus Survey Data

Bayamón Campus Survey Data - New Students Center Building					
NAD27					
18 22 08.08 N					
66 08 38.53 W					
Azimuth Angle (°)	Minimum Elevation Angle (°)	Azimuth Angle (°)	Minimum Elevation Angle (°)	Azimuth Angle (°)	Minimum Elevation Angle (°)
0	1	120	3.5	240	2.2
5	1.7	125	3.1	245	2.2
10	1.8	130	3.7	250	2.5
15	1.9	135	3.2	255	2
20	1.2	140	3.6	260	2.1
25	1.6	145	3.9	265	2.8
30	2.1	150	4.3	270	2.9
35	2.2	155	5	275	3
40	1.5	160	4.3	280	3.1
45	1.7	165	3.3	285	2
50	4.5	170	2.7	290	1.5
55	4.5	175	3.1	295	1.1
60	4.5	180	3.2	300	1.8
65	4.5	185	3	305	1.2
70	4.5	190	4.2	310	1.5
75	2	195	3.1	315	1.6
80	1.9	200	3.5	320	1.3
85	2.1	205	4.3	325	2
90	2.6	210	2.8	330	3.8
95	2.3	215	3	335	1.7
100	2.5	220	2.8	340	1.6
105	3.1	225	2.8	345	2.1
110	3	230	2.4	350	2
115	3.2	235	2	355	1.6

Table B.3. Bayamón Campus Survey Data

Carolina Campus Survey Data - Natural Sciences Laboratories Building					
NAD27					
18 23 00.45 N					
65 59 00.42 W					
Azimuth Angle (°)	Minimum Elevation Angle (°)	Azimuth Angle (°)	Minimum Elevation Angle (°)	Azimuth Angle (°)	Minimum Elevation Angle (°)
0	1.2	120	6.1	240	10.7
5	4.7	125	8	245	9
10	6.5	130	8.4	250	10.6
15	1.2	135	8.1	255	9.5
20	1.3	140	10.9	260	5.3
25	1.5	145	11.8	265	2.4
30	1.2	150	11.7	270	1.7
35	0.9	155	11.9	275	1.4
40	1.4	160	13.7	280	1.1
45	1.4	165	11.4	285	1.1
50	1.6	170	11	290	1.2
55	1.2	175	11.4	295	1.3
60	1.4	180	10.9	300	1.8
65	1.8	185	11.4	305	4.5
70	2	190	12	310	1.7
75	1.9	195	12.3	315	1.1
80	2	200	12.8	320	1.4
85	1.6	205	14.1	325	0.8
90	3.2	210	11.8	330	1.2
95	3.2	215	11.6	335	1.4
100	2.8	220	11.9	340	1.1
105	3	225	9.6	345	1.1
110	4.1	230	10	350	1.1
115	6.1	235	8.9	355	1.1

Table B.4. Carolina Campus Survey Data

Cayey Campus Survey Data - Miguel Melendez Muñoz Sciences Building					
NAD27					
18 07.084 N					
66 09.763 W					
Azimuth Angle (°)	Minimum Elevation Angle (°)	Azimuth Angle (°)	Minimum Elevation Angle (°)	Azimuth Angle (°)	Minimum Elevation Angle (°)
0	13.9	120	6.4	240	6.8
5	14	125	5.9	245	5
10	14.7	130	5.7	250	4
15	16	135	6.5	255	3.9
20	14.6	140	7	260	4.5
25	15.2	145	6.4	265	3.9
30	14.5	150	6.5	270	3.7
35	12.7	155	7.4	275	6.6
40	10.7	160	6.8	280	9.6
45	10.2	165	7	285	9.7
50	8	170	6.8	290	8.7
55	7.7	175	7.2	295	8.4
60	5.1	180	7.4	300	9.5
65	3.9	185	7.6	305	11
70	4	190	8.2	310	11.7
75	5.1	195	8.3	315	11.3
80	5	200	8.8	320	12.3
85	4.7	205	8.2	325	12.8
90	5.3	210	8.1	330	12.2
95	4.7	215	18	335	13
100	3.8	220	8.1	340	11.9
105	4.5	225	6.6	345	12.3
110	5.9	230	5.7	350	13
115	5.6	235	6	355	13.1

Table B.5. Cayey Campus Survey Data

Humacao Campus Survey Data - Library Building					
NAD27					
18 08 43.42 N					
65 50 19.70 W					
Azimuth Angle (°)	Minimum Elevation Angle (°)	Azimuth Angle (°)	Minimum Elevation Angle (°)	Azimuth Angle (°)	Minimum Elevation Angle (°)
0	3.9	120	4.3	240	1.1
5	4.1	125	3.7	245	1.1
10	4.7	130	5.5	250	2.7
15	4.7	135	5.5	255	1.5
20	3.3	140	5.1	260	2.2
25	3	145	4.5	265	2.4
30	4	150	5	270	2.6
35	3.8	155	4.1	275	2.5
40	4.2	160	3.9	280	3.1
45	4.2	165	5.9	285	3.3
50	3.8	170	6	290	3.3
55	3.8	175	5.6	295	4.2
60	4.6	180	5.8	300	5
65	5.4	185	5.4	305	3.9
70	4.9	190	5.2	310	4.5
75	5.5	195	5.4	315	4.4
80	5.5	200	4.8	320	4.4
85	4.6	205	4.8	325	5.5
90	5.2	210	2.9	330	4.1
95	4.4	215	2.4	335	4.9
100	4.1	220	1.9	340	5.7
105	4.1	225	1.4	345	5.6
110	4.6	230	2.1	350	5.3
115	4.1	235	1.1	355	4.3

Table B.6. Humacao Campus Survey Data

Mayagüez Campus Survey Data - Chemistry Building					
NAD27					
18 12 46.33 N					
67 08 27.89 W					
Azimuth Angle (°)	Minimum Elevation Angle (°)	Azimuth Angle (°)	Minimum Elevation Angle (°)	Azimuth Angle (°)	Minimum Elevation Angle (°)
0	3.6	120	1.1	240	3.4
5	3.2	125	1.1	245	3.9
10	3.2	130	1.6	250	4.6
15	2.9	135	1.4	255	3.9
20	2.7	140	1.8	260	3.8
25	2.9	145	1.6	265	4.6
30	2.7	150	2.5	270	4.5
35	2.2	155	2.1	275	4.8
40	2.2	160	1.9	280	4.7
45	2.7	165	1.9	285	3.9
50	1.8	170	2.1	290	3.8
55	1	175	2.6	295	3.7
60	1.1	180	2.4	300	3.8
65	1.1	185	2.5	305	3.7
70	1.1	190	3.1	310	3
75	1.1	195	3.5	315	3.3
80	1.1	200	4.5	320	4.1
85	1.1	205	4.8	325	3.8
90	1.1	210	4.3	330	3.4
95	1.1	215	4.6	335	3.8
100	1.1	220	4.6	340	4
105	1.1	225	4.5	345	3.7
110	1.1	230	3.4	350	2.9
115	1.1	235	3.8	355	2.9

Table B.7. Mayagüez Campus Survey Data

Medical Sciences Survey Data - Central Offices Building					
NAD27					
18 23 41.15 N					
66 04 28.28 W					
Azimuth Angle (°)	Minimum Elevation Angle (°)	Azimuth Angle (°)	Minimum Elevation Angle (°)	Azimuth Angle (°)	Minimum Elevation Angle (°)
0	1.4	120	2.6	240	2.1
5	1.4	125	7.8	245	2.1
10	1.9	130	6	250	2
15	1.2	135	6	255	1.7
20	1.2	140	7.8	260	1.5
25	71.5	145	3.3	265	1.4
30	1.5	150	3.5	270	1
35	2.9	155	2.9	275	1.4
40	1.2	160	2.8	280	1.4
45	1.6	165	2.5	285	1.5
50	2.8	170	2.9	290	7.9
55	1.6	175	3	295	4.6
60	1.7	180	2.4	300	6
65	2.1	185	2.6	305	6
70	1.2	190	2.4	310	6
75	75.9	195	2.3	315	6
80	2.3	200	3.3	320	6
85	1.5	205	3	325	6
90	1.6	210	8.6	330	6
95	2	215	2.2	335	6
100	2.3	220	2.6	340	8
105	2.4	225	2.3	345	6
110	2.3	230	2.7	350	1.4
115	2.4	235	2.7	355	1.4

Table B.8. Medical Sciences Campus Survey Data

Ponce Campus Survey Data - Library Building					
NAD27					
17 59 36.34 N					
66 36 23.61 W					
Azimuth Angle (°)	Minimum Elevation Angle (°)	Azimuth Angle (°)	Minimum Elevation Angle (°)	Azimuth Angle (°)	Minimum Elevation Angle (°)
0	4	120	3.2	240	1.4
5	3.8	125	1.1	245	1.1
10	4	130	2.6	250	1.5
15	4.2	135	2.7	255	1.7
20	4.2	140	3.8	260	1.2
25	4	145	2.5	265	1.4
30	7.6	150	2.9	270	1.5
35	6.7	155	2.3	275	2.3
40	3.6	160	4	280	2.6
45	4	165	1.6	285	3.4
50	5	170	1.8	290	4.1
55	3.3	175	4.4	295	3.6
60	2.9	180	2	300	2.7
65	3.3	185	1.4	305	2.8
70	3.6	190	1.7	310	3.4
75	2.2	195	2	315	4.3
80	3.1	200	1.9	320	4.3
85	1.9	205	2.1	325	4.5
90	3.3	210	1.3	330	4.8
95	2.2	215	5.6	335	5.2
100	3.8	220	6	340	5
105	2.1	225	7.4	345	5
110	2.4	230	6.4	350	4.5
115	2.8	235	5.8	355	3.9

Table B.9. Ponce Campus Survey Data

Rio Piedras Campus Survey Data - North Tower					
NAD27					
18 24 02.70 N					
66 03 08.95 W					
Azimuth Angle (°)	Minimum Elevation Angle (°)	Azimuth Angle (°)	Minimum Elevation Angle (°)	Azimuth Angle (°)	Minimum Elevation Angle (°)
0	1.2	120	3	240	1.6
5	1.4	125	3.3	245	1.4
10	1	130	3.3	250	8.7
15	1.5	135	2.7	255	1.2
20	1.2	140	3	260	1.4
25	1.9	145	3.3	265	1.1
30	1.3	150	2.5	270	1.1
35	1.2	155	2.6	275	0.8
40	1	160	3.3	280	0.8
45	0.8	165	2.6	285	0.8
50	1	170	2.3	290	0.8
55	1.3	175	2.4	295	0.8
60	1.1	180	2.5	300	1.4
65	1.9	185	1.9	305	0.8
70	1.6	190	2.5	310	0.9
75	1.6	195	2.5	315	1.2
80	2.2	200	2.4	320	1
85	1.6	205	2.2	325	0.8
90	1.6	210	2.2	330	1.3
95	1.5	215	2.4	335	0.8
100	1.7	220	2.3	340	0.8
105	1.8	225	1.9	345	0.8
110	1.4	230	1.6	350	0.8
115	2.6	235	1.7	355	0.8

Table B.10. Río Piedras Campus Survey Data

Utua Campus Survey Data - Building B					
NAD27					
18 15.209 N					
66 43.312 W					
Azimuth Angle (°)	Minimum Elevation Angle (°)	Azimuth Angle (°)	Minimum Elevation Angle (°)	Azimuth Angle (°)	Minimum Elevation Angle (°)
0	7.3	120	9.3	240	3.7
5	5.9	125	9.8	245	3.8
10	6.5	130	11	250	5.1
15	6.3	135	11.1	255	5.6
20	6.5	140	10.2	260	5.4
25	8.4	145	8.3	265	5.9
30	8.7	150	6.6	270	5.5
35	8.3	155	5.2	275	5.3
40	7.5	160	5.4	280	5
45	7.7	165	5.8	285	5.2
50	6.3	170	7.9	290	4.8
55	6.6	175	8	295	4.4
60	6.7	180	5.8	300	4.5
65	7.8	185	5.9	305	4.4
70	8.1	190	6.6	310	4.6
75	8.6	195	6.9	315	4.2
80	8.5	200	7	320	3.8
85	7.6	205	7.3	325	4.2
90	8.4	210	7.2	330	3.8
95	8.9	215	7.3	335	5.1
100	10.1	220	7.6	340	5.8
105	11.3	225	6.2	345	5.7
110	9.7	230	5.7	350	5.8
115	8.7	235	4.5	355	5.8

Table B.11. Utua Campus Survey Data

APPENDIX C
RADAR PARTS SPECIFICATIONS SUMMARY

Complete Estimated Radar Cost (Without Scanning System)					
QTY.	Part	Manufacturer	Model	Unit Price	Total
1	Antenna	Seavey Engineering Associates, Inc.	AS48-9494/A	\$ 6,700.00	\$ 6,700.00
1	Orthomode Transducer	Seavey Engineering Associates, Inc.	9951-830	\$ 3,850.00	\$ 3,850.00
1	Magnetron	New Japan Radio Company	M1458	\$ 495.00	\$ 495.00
1	HV Modulator	Pulse Systems, Inc.	/	\$12,500.00	\$12,500.00
1	Magic Tee	Waveline, Inc.	658	\$ 745.00	\$ 745.00
2	Circulator	New Japan Radio Company	NJC3901RB	\$ 65.00	\$ 130.00
2	Crossguide Directional Coupler	Waveline, Inc.	670-SMAF	\$ 745.00	\$ 1,490.00
2	Directional Coupler	Miteq, Inc.	CD-702-1242-20S	\$ 120.00	\$ 240.00
2	TR Limiter	New Japan Radio Company	TL393	\$ 409.00	\$ 818.00
2	Double-Throw Switch	Miteq, Inc.	N247B	\$ 425.00	\$ 850.00
2	Low Noise Front End	Miteq, Inc. or Waveline, Inc.	ARZ0227	\$ 6,375.00	\$12,750.00
1	10 MHz Master Oscillator	Wenzel Associates, Inc.	500-10660	\$ 1,965.00	\$ 1,965.00
1	Phase Locked Oscillator	Communication Techniques, Inc.	XPDR0-93XX	\$ 1,250.00	\$ 1,250.00
2	Power Divider	Mini-Circuits	ZFSC-2-1W	\$ 48.95	\$ 97.90
1	Power Divider	Miteq, Inc.	D0258	\$ 180.00	\$ 180.00
2	Switch	Mini-Circuits	ZASWA-2-50DR	\$ 89.95	\$ 179.90
2	Attenuator	Mini-Circuits	BW-S12W5	\$ 44.95	\$ 89.90
4	Attenuator	Mini-Circuits	BW-S40W5	\$ 44.95	\$ 179.80
2	Mixer	Mini-Circuits	ZX05-1LHW	\$ 38.95	\$ 77.90
2	Directional Coupler	Mini-Circuits	ZFDC-20-5	\$ 84.95	\$ 169.90
2	Amplifier	HD Communications Corp.	HD19012	\$ 1,055.00	\$ 2,110.00
2	Amplifier	HD Communications Corp.	HD19153	\$ 1,055.00	\$ 2,110.00
2	Low Pass Filter	Mini-Circuits	SLP-30	\$ 34.95	\$ 69.90
4	Band Pass Filter	Lark Engineering Company	XMC10-7-5AA	\$ 172.00	\$ 688.00
4	Schottky Diode Detector	Agilent Technologies	8472B	\$ 626.00	\$ 2,504.00
1	8 Bits Digitizer	National Instruments	NI PXI-5102	\$ 1,495.00	\$ 1,495.00
1	CPU Module/Processor	PC/104 Embedded Consortium	CMG7686GX300-3V-128	\$ 2,000.00	\$ 2,000.00
1	Direct Digital Synthesis	Analog Devices, Inc.	AD9854	\$ -	\$ -
1	D/A	PC/104 Embedded Consortium	AX10415	\$ 210.00	\$ 210.00
1	Voltage Controlled Oscillator	Mini-Circuits	ZOS-50	\$ 119.95	\$ 119.95
1	DSP Board/Controllers	GV & Associates, Inc.	GVA-290	\$20,000.00	\$20,000.00
Estimated Radar Cost					\$76,065.15

Table C.1. Radar parts specifications summary